Temporal and Geochemical Variability of Volcanic Products of the Marquesas Hotspot

D. L. DESONIE[1] AND R. A. DUNCAN

College of Oceanic and Atmospheric Sciences, Oregon State University, Corvallis

J. H. NATLAND[2]

Scripps Institution of Oceanography, University of California, La Jolla

The Marquesas archipelago is a short, NW-SE trending cluster of islands and seamounts that formed as a result of volcanic activity over a weak hotspot. This volcanic chain lies at the northern margin of a broad region of warm and compositionally diverse mantle that melts to build several other subparallel volcanic lineaments. Basalts dredged from submerged portions of volcanoes along the Marquesas lineament decrease in age from northwest to southeast. The new sample age distribution yields a volcanic migration rate significantly slower than that expected for Pacific plate motion over a stationary Marquesas hotspot. This and the aberrant orientation of the chain indicate deflection of the plume by westward upper mantle flow. The interaction of this weak plume with upper mantle flow accounts for the temporal and spatial patterns in Marquesan volcanism. The compositions of subaerial and submarine basalts reflect the mixing of at least two mantle sources, distinguished by Sr, Nd, and Pb isotope and trace element compositions. There is a consistent evolutionary pattern at each volcano, from early tholeiitic to later alkalic basalt eruptions. Tholeiitic and transitional lava compositions can be derived by variable degrees of partial melting of a source composed of depleted mid-ocean ridge basalt mantle (DMM) and mantle characterized by radiogenic Pb (HIMU). Alkalic lava compositions appear to be dominantly the result of smaller degrees of melting of a more radiogenic mantle source (EM II). Large-scale melting of the lower lithosphere or upper mantle (DMM+HIMU) entrained within a sheared, thermally buoyant plume (EM II) could produce the tholeiitic and transitional basalts found in the main shields of the volcanoes, while alkalic basalts could result from melting of mantle of EM II composition at the edges of the hotspot.

THE MARQUESAS VOLCANIC LINEAMENT

The Marquesas lineament, the northernmost of the many hotspot lineaments of French Polynesia, includes 12 islands and at least eight seamounts that extend for nearly 500 km north of the Marquesas Fracture Zone (Figure 1). These youthful volcanic cones rise up to 5000 m from 50- to 65-m.y.-old oceanic lithosphere [*Kruse*, 1988] that formed at the ancestral East Pacific Rise (EPR). The Marquesas, and the other islands of French Polynesia, are on the western side of an unusually shallow region of thinner than normal lithosphere, termed the South Pacific isotopic and thermal anomaly (SOPITA), thought to be a zone of broad-scale mantle upwelling [*McNutt and Fischer*, 1987; *Smith et al.*, 1989; *McNutt and Judge*, 1990; *Staudigel et al.*, 1991]. Extreme compositional variations are found for basalts on a variety of scales: between and among island groups, and within individual volcanoes [*Bishop and Woolley*, 1973; *Liotard et al.*, 1986; *Duncan et al.*, 1986; *Vidal et al.*, 1987]. Volcanism above the Marquesas hotspot has been intermittent, is somewhat oblique to volcanism at other south Pacific lineaments [*Crough and Jarrard*, 1981], and is the only French Polynesian hotspot track for which there is no known site of active volcanism.

In this paper we report new ^{40}Ar-^{39}Ar and K-Ar age determinations from eight dredge hauls and the island of Fatu Hiva in the Marquesas lineament, which revise the age progression previously determined from studies of island samples only. Major and trace element contents are consistent with fractional crystallization from a range of primary basalt melt compositions. Isotopic ratios identify the parental mantle compositions as having depleted mid-ocean ridge basalt mantle plus mantle characterized by radiogenic Pb (DMM+HIMU) and more radiogenic mantle source (EM II) signatures, in *Zindler and Hart's* [1986] terminology. We discuss these data in terms of possible dynamic models of mantle plume and lithosphere/asthenosphere melting and mixing.

Age Relationships of Marquesas Volcanoes

Previous results of K-Ar age determinations from the islands of the Marquesas [*Duncan and McDougall*, 1974; *Duncan et al.*, 1986; *Brousse et al.*, 1990] have shown a southeastward migration of volcanism along the Marquesas chain from 6 Ma at Eiao [*Brousse et al.*, 1990; *Caroff et al.*, 1990] through 1.3 Ma at Fatu Hiva [*Duncan and McDougall*, 1974]. The resultant volcanic migration rate of 104 ± 18 km/m.y. closely matches those calculated for other French Polynesian volcanic chains [*McDougall and Duncan*, 1980].

It has been suggested that volcanism over the Marquesas hotspot did not initiate at Eiao (Figure 1). Volcanism at ridges to the west of the Marquesas Islands along the Galapagos Fracture Zone and the Nova-Canton trough, with ages of 13 and 30 Ma, respectively, has been proposed to have originated
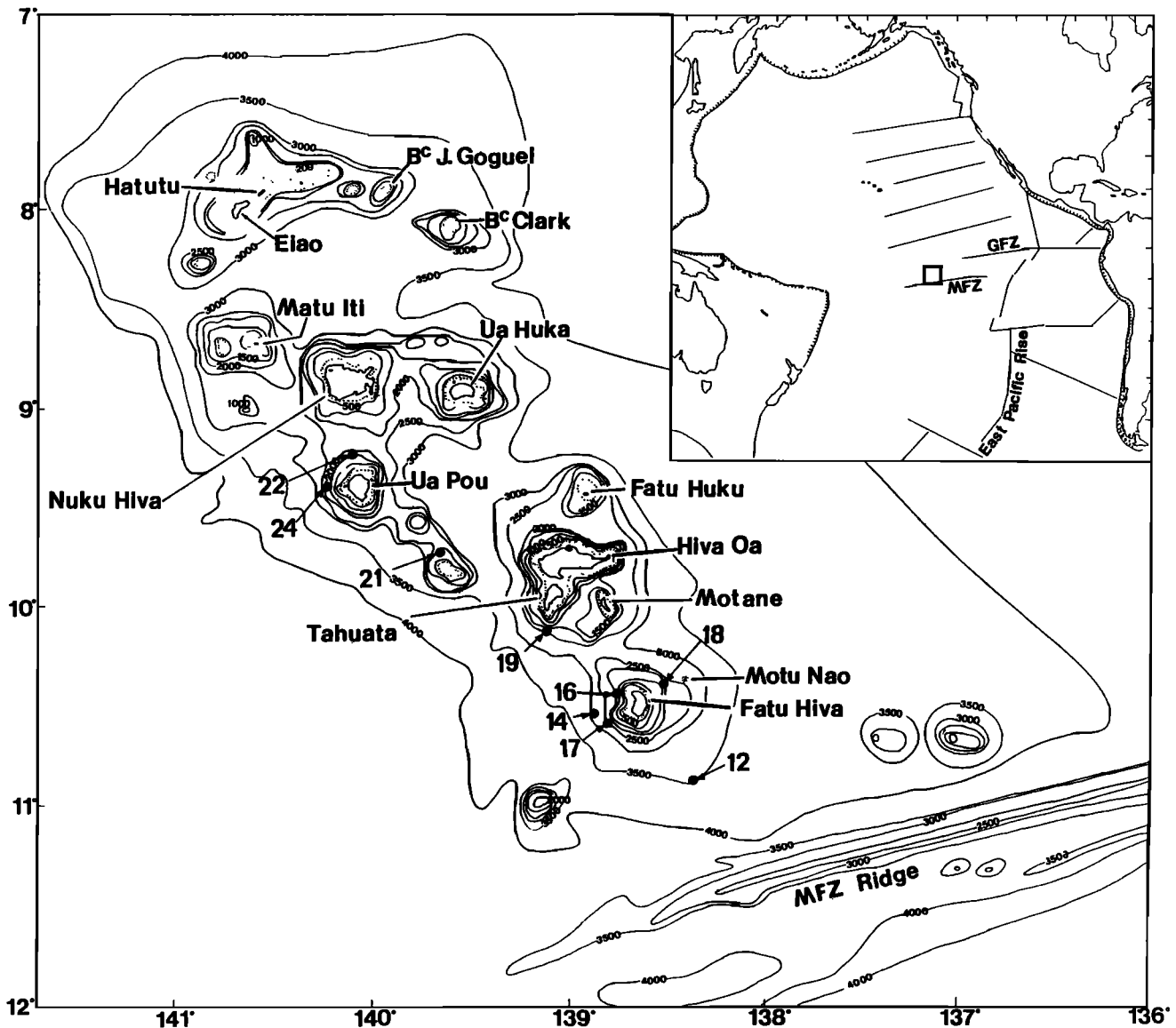
Fig. 1. Bathymetric map of the Marquesas lineament. Arrows indicate locations of dredge hauls; after GEBCO Map 297, Centre National pour l'Exploitation des Oceans, Paris, 1973. Contour interval = 500 m, dotted line contour = 200 m. Insert indicates the location of the Marquesas bathymetric map and shows major tectonic features of the Pacific Ocean basin: Galapagos Fracture Zone (GFZ), Marquesas Fracture Zone (MFZ), and the East Pacific Rise.

over the Marquesas hotspot [*McNutt et al.*, 1989]. A long, broad topographic and geoid swell extends westward from the Marquesas lineament through the center of the north-south trending Line Islands volcanic lineament. This feature, termed the Line-Cross trend, has allowed speculation that at least some of the central Line Islands formed above the Marquesas hotspot [*Crough and Jarrard*, 1981]. Three of the volcanoes, with ages between 38 and 60 Ma, show an age progression which could be related to volcanism along the Marquesas-Line trend [*Schlanger et al.*, 1984]. If so, the Marquesas hotspot has produced volcanic activity only intermittently.

In contrast to the three other volcanic chains of the French Polynesian region (Society, Austral-Cook, Pitcairn-Gambier), no active volcanism has been found at the southeastern end of the Marquesas line [*McNutt et al.*, 1989]. *McNutt et al.* [1989] proposed that the most recent expression of volcanism above the Marquesas hotspot may be found at the northern ridge

margin of the Marquesas Fracture Zone (MFZ). Further study of this ridge has shown that it is an old feature unrelated to hotspot activity (M. K. McNutt, personal communication, 1991). In September 1991, however, fresh glassy basalts were dredged from a seamount at the southeast end of the Marquesas lineament, 20 km north of the MFZ, now thought to be the present location of the hotspot (M. K. McNutt, personal communication, 1991); radiometric ages for these samples are in progress (R. A. Duncan, unpublished results, 1993).

The duration of volcanism at a single edifice within this lineament is longer than that measured at other hotspot locations. *Duncan et al.* [1986] discovered that the 3.8-m.y. history of volcanism at the island of Ua Pou followed a petrogenetic sequence similar to Hawaiian volcanoes. Shield lavas exposed in stream valleys, road cuts and wave-cut cliffs around the perimeter of Ua Pou are part of a tholeiitic basalt phase of volcanism which occurred from 5.6 to 4.5 Ma.

Volcanism began again after a 1.6 m.y. hiatus with eruption of alkali basalts from 2.9 to 2.7 Ma, and finally more evolved lavas from 2.5 to 1.8 Ma [*Duncan et al.*, 1986]. In contrast with Hawaiian volcanism, the magmatic production rate is independent of composition and does not diminish with time, based on the age relationships of the compositional phases on each of the Marquesan volcanoes [*Brousse et al.*, 1990].

Geochemical Variability of SOPITA Volcanic Chains

The south-central Pacific basin presents several remarkable geochemical and geophysical characteristics. This region (essentially French Polynesia) has thinner lithosphere [*Nishimura and Forsyth*, 1985] and shallower depths [*McNutt and Fischer*, 1987] than comparably old lithosphere elsewhere. Slow lower mantle seismic velocities [*Dziewonski and Woodhouse*, 1987] directly beneath the region correlate with an unusually high density of hotspot tracks. These volcanoes exhibit some of the most extreme isotopic compositions among oceanic basalts [*Duncan and Compston*, 1976], which *Hart* [1984] and *Castillo* [1988] have related to large-scale convective upwelling from the deep mantle. *Staudigel et al.* [1991] have shown that the compositional identity of the volcanism has persisted at least since mid-Cretaceous time and speculated that the diversity in the island and seamount basalts is derived from long-term accumulation and isolation of subducted lithosphere deep in the mantle. In this interpretation, recycled material is delivered to the upper mantle beneath the region via plume flow [*White and Hofmann*, 1982]. The Darwin Rise [McNutt and Judge, 1990] and the western Pacific Cretaceous atoll and guyot province [*Smith et al.*, 1989] probably originated over hotspots in this area. The term "superswell" has been used to describe this broad, shallow region of the Pacific correlated with deep mantle upwelling and excess intraplate volcanism [*McNutt and Fischer*, 1987].

Within the four volcanic lineaments of French Polynesia are some of the most extreme Sr and Pb isotopic compositions yet measured in ocean island basalts (OIB). The mantle components visualized as endmember source compositions in globally distributed oceanic volcanism [*White*, 1985; *Zindler and Hart*, 1986] must have developed from long-term isolation of materials with variable U/Pb, Th/Pb, Rb/Sr and Sm/Nd; these are well represented in south-central Pacific lavas. Figure 2 shows spreading ridge and hotspot lavas from the region plotted in $^{87}Sr/^{86}Sr$ - $^{206}Pb/^{204}Pb$ space with hypothesized mantle endmember compositions. DMM, depleted mid-ocean ridge basalt (MORB) mantle, is the low radiogenic Sr and Pb, globally quite uniform, endmember that gives rise to normal spreading ridge lavas. HIMU, the radiogenic Pb, unradiogenic Sr component, was defined in part by basaltic rocks from Mangaia and Tubuai in the Cook-Austral Islands, and appears to be present in Easter Island lavas and seafloor basalts from the EPR. EM II, with highly radiogenic Sr but moderate $^{206}Pb/^{204}Pb$, is most evident in samples from Samoa but is also strongly expressed in lavas from the Society and the Marquesas Islands. EM I component, with moderately high $^{87}Sr/^{86}Sr$ but low $^{206}Pb/^{204}Pb$ is represented by samples from Pitcairn Island and Rarotonga in the Cook Islands.

Compositional diversity is observed along and across lineaments, and on the scale of individual volcanoes. In the Cook-Austral lineament islands exhibit rather uniform compositions, whereas great isotopic diversity is found between volcanoes (Figure 2). In the Marquesas lineament
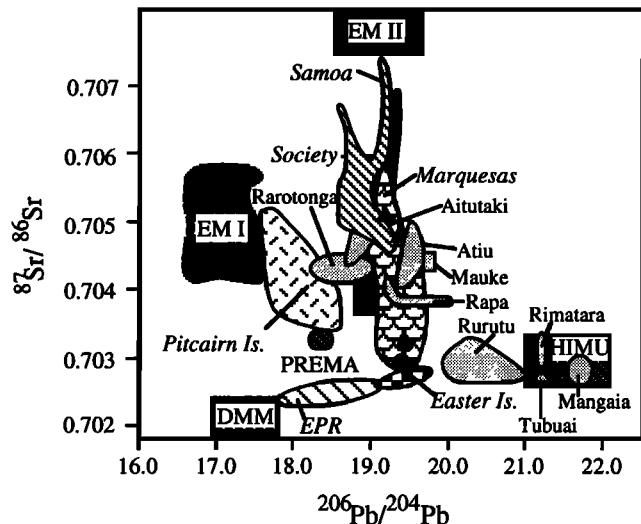
Fig. 2. $^{87}Sr/^{86}Sr$ versus $^{206}Pb/^{204}Pb$ for south Pacific spreading ridge basalts and hotspot volcanic lineaments with mantle components after *Zindler and Hart* [1986] shown in hatchured boxes. Although data from most island chains are grouped, data from each volcano in the Cook-Austral lineament is shown as a separate field but with the same dotted pattern and print. Basalts from the island of Ua Pou [*Duncan et al.*, 1986] are tholeiitic basalts (solid circles) and alkalic basalts (solid triangles). Data sources are as follows: East Pacific Rise (EPR) [*White et al.*, 1987]; Easter Island [*White and Hofmann*, 1982]; Society Islands [*White and Hofmann*, 1982; *Cheng et al.*, 1987; *Devey et al.*, 1990; W. M. White, unpublished data, 1990]; Marquesas Islands [*Vidal et al.*, 1984; *Duncan et al.*, 1986; *Dupuy et al.*, 1987; *Desonie*, 1990]; Cook and Austral Islands [*Palacz and Saunders*, 1986; *Nakamura and Tatsumoto*, 1988]; Pitcairn Island [*Woodhead and McCulloch*, 1989]; and the Samoan Islands [*Wright and White*, 1986; *Farley et al.*, 1990]; after *Hart and Zindler* [1989].

extreme heterogeneity is found within a single volcano. The quartz-normative tholeiites from Ua Pou are among the most depleted in $^{87}Sr/^{86}Sr$ for ocean islands yet found, but they have consistently higher Pb-isotope ratios than MORB. The more radiogenic Pb-isotope ratios of these tholeiites may be due to the incorporation of pods of a HIMU component within the DMM mantle source [*Duncan et al.*, 1986; Hart and Zindler, 1989]. Alkalic lavas from the same volcano, however, are intermediate in Pb isotopic compositions and have highly radiogenic Sr isotopic ratios, characteristic of an EM II source composition (Figure 2).

The spatial variability of melt compositions across the hotspots can be examined through sampling of contemporaneous volcanoes within the region of current activity. In the group of young volcanoes at the southeast end of the Societies chain, between Tahiti and Mehetia, an isotopic gradient in $^{87}Sr/^{86}Sr$ perpendicular to the hotspot track is found in which values of 0.7060 at Rocard seamount to the north, decrease to values of 0.7031 at Moua Pihaa seamount to the south [*Devey et al.*, 1990]. Isotopic gradients in the direction of plate motion are also observed. For example, as mentioned above, at the island of Ua Pou, tholeiitic basalts ($^{87}Sr/^{86}Sr$ = 0.7027) predate alkalic basalts ($^{87}Sr/^{86}Sr$ = 0.7055) by ≥ 1.5 m.y. Given the high plate velocities inferred from Pacific volcano migration rates [*Duncan and Clague*, 1985], this implies a sample spacing of 100 to 150 km across the hotspot. *Duncan et al.* [1986] suggested that the composition of the eruptive products at Ua Pou was related to position of the volcano above a compositionally segregated hotspot.

NEW RESULTS FROM THE MARQUESAS ISLANDS AND SWELL

Samples and Analytical Methods

Basalt samples examined in this study were dredged from submarine portions of the Marquesas volcanic chain in March and April of 1987 by the R/V Thomas Washington, expedition Crossgrain (CRGN 02). The objectives of the program were twofold: to study the thermo-mechanical properties of the lithosphere underlying the Marquesas lineament and to determine the chemical composition of the early phase of construction of the volcanoes. A portion of the results of Sea Beam swath mapping, a single channel seismic study, and gravity and magnetic surveys were discussed by *McNutt et al.* [1989] and *Filmer and McNutt* [1990].

In this paper we report analyses of rocks recovered in nine dredge hauls of seamounts, banks, and the submarine portions of islands from CRGN 02. Dredge locations from which basaltic rocks were recovered are shown in Figure 1 and brief descriptions of the dredge targets are given in Table 1. Previous studies of Marquesan volcanism have relied solely on samples from the emergent portions of the volcanoes which represent less than 2% of the mass of any edifice.

For petrologic comparison of dredged lavas and glasses with those from emergent portions of the islands, initial basalt classifications are those used by *Liotard et al.* [1986], following *Feigenson et al.* [1983] for Hawaiian basalts. Hypersthene-normative basalts are classified as tholeiitic if they lie in the tholeiitic field on an alkalis versus silica plot and as transitional if they lie in the alkalic field. All nepheline-normative samples are alkalic basalts. Although all three compositional types are represented in the CRGN 02 sample suite (Tables 4 and 5), highly alkalic rocks (>30% normative nepheline), which are abundant among subaerial samples, were not recovered. Rock names were then given to members of each of these lava types using the International Union of Geological Sciences classification based on their major and trace element compositions, and normative and modal mineralogies. Glasses were named based on their position on an alkalies versus silica diagram.

The dredge hauls contained glasses and well-crystallized rocks. In general, the dredged material provided the same rock types found on the islands; most individual dredges collected rocks of essentially uniform composition. For example, nearly identical ages and compositions from all analyzed samples from DH 12 indicate that only one flow sequence was sampled. A few dredge hauls contained a greater variety of rock types. The most diverse, DH 19, from a fault scarp on the south side of the island of Tahuata, returned olivine tholeiites (19-1,

19-2), alkali basalts (19-3, 19-11), and one basanite (19-8). The diversity of compositions from this sample site is similar to that observed on the island of Ua Pou. Hyaloclastites were dredged from three locations (DH 17, DH 18, and DH 21).

Samples used for age determinations and compositional analyses were the freshest available, with slight to moderate alteration and little or no interstitial glass. All CRGN 02 samples, except the potassic trachyandesites, are highly vesicular. Tholeiitic basalts include olivine (some embayed) and abundant clinopyroxene phenocrysts. Fe-Ti oxides, clinopyroxene, and small amounts of interstitial glass are found in the groundmass. Basalts (transitional series) are similar to olivine tholeiites but include small laths of groundmass plagioclase. Abundant embayed olivine crystals are found as phenocrysts and in the groundmass of alkali olivine basalts. Augitic clinopyroxene is abundant as well. Although DH 21 samples are classified chemically as alkali olivine basalts, they contain no olivine, little clinopyroxene and have abundant small plagioclase laths in a trachytic matrix. The highly vesicular tephrites contain abundant clinopyroxene (rhomboid phenocrysts), and some olivine. Little or no plagioclase is found in the tephritic rocks. Basanites are fine grained with abundant olivine, clinopyroxene, and plagioclase phenocrysts and microphenocrysts. Vesicles in the basanitoids are extremely round, and up to 1 mm in diameter. Highly alkalic samples contain abundant titanaugite which is sometimes sector zoned with normally and reversely zoned rims. Potassic trachyandesites contain fine grained plagioclase laths, minor clinopyroxene and Fe-Ti oxides in a trachytic matrix.

Age determinations by ^{40}Ar-^{39}Ar incremental heating and total fusion experiments and conventional K-Ar radiometric dating methods were performed on 23 fresh basalt samples from the CRGN 02 dredge collection and six samples from the island of Fatu Hiva. Sample preparation and analysis of samples by K-Ar and ^{40}Ar-^{39}Ar total fusion methods followed the techniques outlined by *Desonie and Duncan* [1990]. Experimental methods for ^{40}Ar-^{39}Ar incremental heating are described by *Duncan and Hargraves* [1990]. Air measurements to determine the mass discrimination factor, critical to correction for atmospheric argon, were performed after each two sample runs for total fusion analyses and before each stepwise heating experiment.

Because of the potential for potassium addition and argon loss in seawater, K-Ar analyses on crystalline submarine volcanic rocks provide only a minimum age. ^{40}Ar-^{39}Ar incremental heating experiments can provide a reliable crystallization age if a plateau in the age versus temperature spectrum is formed and appropriate statistical criteria are met.

TABLE 1. Location and Description of CRGN 02 Dredge Hauls in Which Basaltic Rocks Were Recovered

Station	Latitudes, °S	Longitudes, °W	Depth, m	Feature
DH 12	10°49.1'	138°25.9'	2985-3136	small seamount 50 km southeast of Fatu Hiva
DH 14	10°32.3'	138°50.8'	2442-2077	scarp in basal dome west of Fatu Hiva
DH 16	10°26.0'	138°45.8'	2307-1936	N-S trending scarp basal dome west of Fatu Hiva
DH 17	10°31.5'	138°48.7'	2437-2348	scarp in basal dome southwest of Fatu Hiva
DH 18	10°23.8'	138°32.2'	1992-1758	southwest flank of Motu Nao
DH 19	10°05.9'	139°08.8'	1936-1717	flank of N-S trending ridge 6 km south of Tahuata
DH 21	9°39.6'	139°43.7'	2524-2296	west flank Dumont D'Urville Nord rift zone
DH 22	9°13.6'	140°07.6'	2036-1692	small cone on north slope of Ua Pou
DH 24	9°25.2'	140°14.6'	2780-2006	rift zone on steep slope west of Ua Pou

For a plateau to be defined, two contiguous steps with calculated ages within 1σ and representing at least 50% of the total ^{39}Ar released from the sample were required. If three or more steps were used in the calculation an isochron age (^{36}Ar/^{40}Ar versus ^{39}Ar/^{40}Ar) was also calculated. The ^{40}Ar/^{36}Ar intercept in each of these calculations (Table 3) shows no evidence for nonatmospheric, initial argon. (By virtue of the distribution of the few points used in the regressions, three isochrons yielded ^{40}Ar/^{36}Ar intercepts less than the atmospheric value, 295.5, and resulting calculated ages are too old. In these cases we accept the plateau age as the best estimate of the crystallization age.) Because of the expected young ages and only moderate potassium contents in some of these lavas, and thus low amounts of radiogenic ^{40}Ar, ^{40}Ar-^{39}Ar total fusion experiments were done on some dredged samples.

Major and trace element analyses of the dredged basalts were carried out by X ray fluorescence spectroscopy (XRF) using fused glass disks, as described by *Hooper* [1981]. Rare earth element (REE) and Hf concentrations were determined by instrumental neutron activation analysis (INAA) following the method of *Laul* [1979]. Five basalt fragments (14-1, 16-1, 16-2, 16-3, and 19-11), too small for analysis by XRF, were powdered, fused under controlled atmosphere (QFM) and analyzed for major elements by electron microprobe at Oregon State University. Compositions of 13 Marquesan glasses were analyzed by electron microprobe at Scripps Institution of Oceanography (Table 5).

For analyses of radiogenic isotope ratios, 0.5- to 1.0-mm chips of all samples were leached in warm, distilled 6 N HCl for 1 hour to attempt to eliminate effects of seawater alteration. Sr, Nd, and Pb concentrates were then obtained from dissolved powders by ion exchange, and isotopic ratios were measured on a VG Sector thermal ionization mass spectrometer at Cornell University, following the procedure of *White et al.* [1990].

Age Determinations

Analytical data and age calculations from the K-Ar and ^{40}Ar-^{39}Ar total fusion and incremental heating experiments are given in Tables 2 and 3. Figure 3 shows the variation in age of 12 islands and eight dredge sites with distance along the lineament, measured from the position of DH 12. Samples from CRGN 02 expand the age range previously seen at some volcanoes. Because the current location of the Marquesas hotspot relative to the Pacific plate is unknown, we use the location of DH 12 as the youngest point in the Marquesas lineament for plate motion calculations. DH 12 is the most southeasterly location from which ages have been determined; the age of basalts from these seamounts is significantly younger than those from Fatu Hiva.

Because volcanism at a single volcano can last for as much as 3-4 m.y. in the Marquesas [*Duncan et al.*, 1986] and the volcanic record at the various sites has been incompletely sampled, we have calculated the rate of plate motion over the Marquesas hotspot in three ways. For all calculations, the most reliable age determinations available (^{40}Ar-^{39}Ar total fusion or incremental heating for submerged basalts, K-Ar for island samples) were used in a least squares linear regression. In one calculation, the oldest age from each island and dredge location was used. In another analysis, only basalts known to be of tholeiitic or transitional composition, and thus representing a common phase in volcano development, were used. Regression rates for both of these cases, which we take to estimate the time when the individual volcanoes were located over the center of the hotspot, are identical at 74 ± 6 km/m.y.

TABLE 2. K-Ar and ^{40}Ar-^{39}Ar Total Fusion Ages for Basalts From CRGN 02 Dredges and the Island of Fatu Hiva, Marquesas Swell

Sample	% K	^{40}Ar Radiogenic, $\times 10^{-8}$ mol/g	% ^{40}Ar Radiogenic	Age ± 1 σ, Ma
		CRGN 02		
DH 12-1	2.11	3.2	4.4	0.39 ± 0.04
DH 12-10	[n.d.]		4.3	0.35 ± 0.04
	[2.02]		4.5	0.45 ± 0.10
DH 12-11	[2.07]		5.2	0.48 ± 0.10
DH 17-1	1.49	4.9	18.7	0.84 ± 0.03
DH 17-2	[1.14]		9.4	1.31 ± 0.12
DH 18-26	[0.71]		4.1	0.74 ± 0.12
DH 18-40	[n.d.]		4.9	1.27 ± 0.03
DH 19-1	0.73	4.4	6.9	1.57 ± 0.05
	[n.d.]		4.9	1.58 ± 0.08
DH 19-8	2.31	15.8	26.1	1.76 ± 0.10
DH 21-8	[1.12]		11.4	3.13 ± 0.14
DH 21-14	[n.d.]		25.1	2.81 ± 0.04
DH 22-1	1.54	15.0	32.8	2.49 ± 0.04
DH 24-4	2.57	29.6	27.4	2.97 ± 0.04
DH 24-7	2.62	30.2	31.9	2.96 ± 0.03
DH 24-8	[n.d.]		7.8	2.45 ± 0.14
		Fatu Hiva		
FT 01-02	0.95	4.4	6.6	1.18 ± 0.06
FT 01-23	1.41	10.0	5.2	1.84 ± 0.14
FT 01-39	1.47	8.2	5.5	1.43 ± 0.05
FT 01-42	1.47	7.2	17.5	1.24 ± 0.02
FT 01-61	1.02	7.6	7.1	1.91 ± 0.09
FT 01-65	1.07	7.3	5.7	1.76 ± 0.12

Ages calculated using the following decay and abundance constants: $\lambda_\varepsilon = 0.581 \times 10^{-10}$ yr^{-1}; $\lambda_\beta = 4.963 \times 10^{-10}$ yr^{-1}; ^{40}K/K = 1.167×10^{-4} mol/mol. % K determined by atomic absorption spectrophotometry, or calculated from measured ^{39}Ar (in brackets; n.d. = not determined).

TABLE 3. ^{40}Ar-^{39}Ar Plateau and Isochron Ages From CRGN 02 Basalts

Sample	Plateau Age ± 1 σ, Ma		^{39}Ar,	Integrated	Isochron Age,	N	SUMS/(N-2)	^{40}Ar/^{36}Ar
	Weight by 1/σ²	Weight by %^{39}Ar	% of Total	Age, Ma	± 1σ, Ma			Intercept
DH 12-17	0.76 ± 0.10	0.76 ± 0.24	100.0	0.76	0.60 ± 0.05	6	0.3	295.6 ± 2.4
DH 16-1	1.31 ± 0.04	1.28 ± 0.13	94.7	1.22	1.22 ± 0.03	4	0.0	296.5 ± 0.7
DH 17-1	1.70 ± 0.07	1.60 ± 0.20	87.0	1.73	1.54 ± 0.37	5	0.8	283.4 ± 9.9
DH 17-5	1.69 ± 0.11	1.60 ± 0.38	100.0	1.60	1.25 ± 1.52	6	3.1	298.1 ± 11.0
DH 18-13	1.27 ± 0.10	1.29 ± 0.20	67.0	1.92	2.28 ± 0.36	4	1.0	286.2 ± 2.5
DH 19-2	1.74 ± 0.08	1.58 ± 0.23	96.2	1.58	1.85 ± 0.12	3	0.7	291.6 ± 0.5
DH 19-3	1.97 ± 0.12	1.86 ± 0.19	99.4	1.82	-	2	-	-
DH 19-8	1.87 ± 0.05	1.83 ± 0.06	99.4	1.82	1.75 ± 0.18	5	2.4	293.4 ± 2.8
DH 19-11	none developed		_	1.60	-	-	-	-
DH 21-14	2.63 ± 0.19	2.60 ± 0.28	73.8	2.61	-	2	-	-
DH 22-1	2.69 ± 0.07	2.69 ± 0.24	92.3	2.87	-	2	-	-
DH 22-2	3.50 ± 0.08	3.43 ± 0.16	75.2	3.85	3.57 ± 0.12	3	0.2	280.9 ± 4.4
DH 24-4	3.24 ± 0.09	3.36 ± 0.20	81.8	3.12	3.17 ± 0.14	5	1.0	290.1 ± 4.4
DH 24-7	3.28 ± 0.07	3.27 ± 0.17	94.6	3.23	3.03 ± 0.20	5	0.4	296.1 ± 11.9

Corrected for ^{37}Ar decay since irradiation, half-life = 35.1 days. Ages calculated using the following decay and abundance constants: λ_ϵ=0.581x10^{-10} yr^{-1}; λ_β=4.963x10^{-10} yr^{-1}; ^{40}K/K=1.167x10^{-4} mol/mol. Neutron flux monitored with hornblende standard MMhb-1 (520.4 Ma).

These estimates are low relative to those calculated from average volcano ages compiled from all samples for which age determinations have been performed. A third regression of all 140 age determinations [Duncan and McDougall, 1974; Duncan et al., 1986; Katao et al., 1988; Brousse et al., 1990; Desonie, 1990; D. L. Desonie, unpublished data, 1992] leads to a rate of 93 ± 7 km/m.y. This rate is lower than (but within statistical uncertainty) the rate of 104 ± 18 km/m.y. calculated by McDougall and Duncan [1980] who used all island data

available to them in their regression. Regression lines were extrapolated to zero age to determine the current location of the Marquesas hotspot. For the regression rate calculated from the tholeiitic/transitional basalts the current hotspot location is 37 km southeast of DH 12. For the rate calculated for all Marquesan basalts the current hotspot location is 49 km southeast of DH 12. In view of the more complete sampling of these volcanoes and the evidence for a common compositional sequence at each center, we conclude that the most appropriate
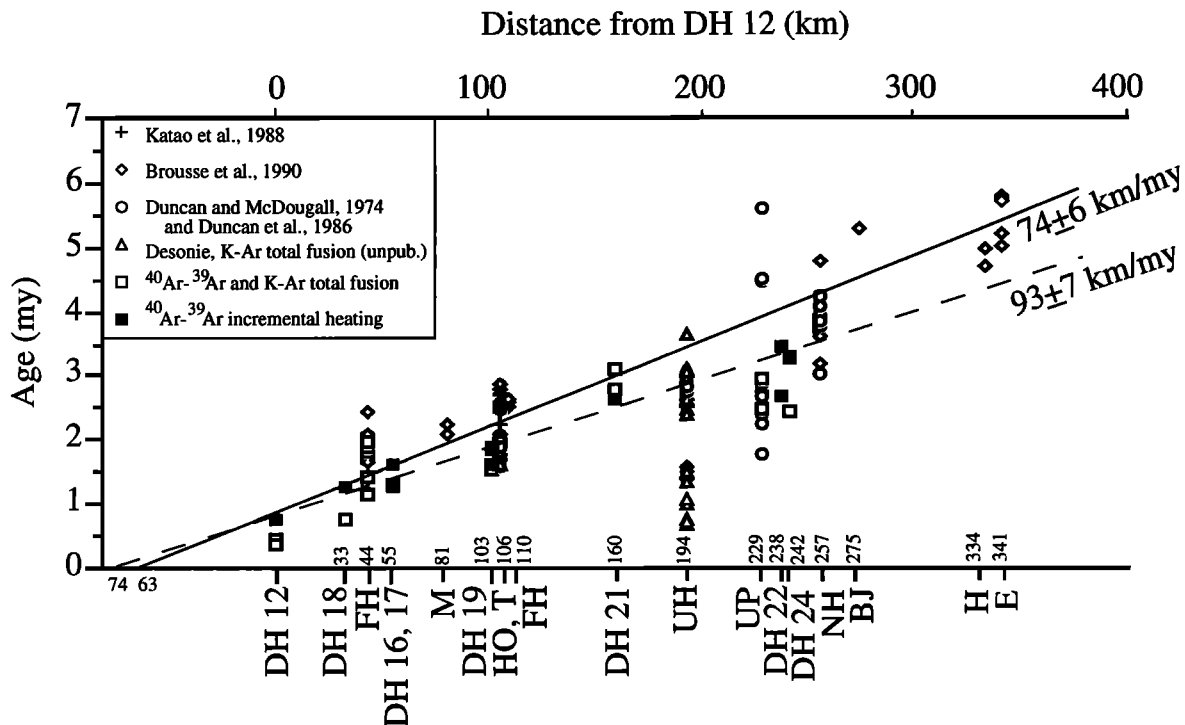

Fig. 3. Basalt age versus distance from DH 12 for seamounts and islands of the Marquesas lineament. Distances are measured along the trend of the Marquesas chain (N40°W). Solid symbols represent rocks analyzed by the ^{40}Ar-^{39}Ar incremental heating technique for which a plateau age was calculated. Open symbols represent data generated by ^{40}Ar-^{39}Ar or K-Ar total fusion experiments. Two least squares regression lines are pictured: one with a slope of 74 km/m.y. calculated from oldest ages at each volcanic center and one with a slope of 93 km/m.y. calculated from all available Marquesas age determinations. A third regression line for all tholeiitic and transitional basalt samples for which ages have been determined, also with a slope 74 km/my, is not pictured. The intercept of each regression line with the x axis shows the predicted present location of the Marquesas hotspot southeast of DH 12. Island locations in this figure and in Figure 12 are indicated by the following symbols: B^c J. Goguel (BJ), Hatutu (H), Eiao (E), Nuku Hiva (NH), Ua Huka (UH), Ua Pou (UP), Fatu Huku (FH), Hiva Oa (HO), Tahuata (T), Motane (M), and Fatu Hiva (FH).

velocity for Pacific plate motion over the Marquesas hotspot is our new estimate of 74 km/m.y. We later discuss implications for motion of the Marquesas hotspot with respect to other Pacific hotspots.

DH 19 is the only dredge haul that contains representatives of tholeiitic, transitional, and alkalic magma types. Lack of stratigraphic information from dredge sampling does not allow relative position of the three compositional phases of volcanism to be known. Ages of each of the three phases of volcanism can be compared with the sequence found on Ua Pou where tholeiitic shield lavas predate alkalic cap rocks [*Duncan et al.*, 1986]. The youngest samples from DH 19 are tholeiitic (19-1: 1.58 ± 0.08 Ma; 19-2: 1.70 ± 0.08 Ma), but the ages are similar to ages from transitional (19-3: 1.97 ± 0.12 Ma) and alkalic (19-8: 1.87 ± 0.03 Ma) basalts. Although at Ua Pou a distinct age versus composition relationship is seen, samples from DH 19 show that the two compositional types sometimes overlap in time, perhaps especially during the submarine construction of the volcanoes.

New samples were also collected from the emergent portion of the island of Fatu Hiva during the CRGN 02 expedition. Age determinations, performed by K-Ar methods, expand the age range previously seen at that edifice and are included in Table 2. Compositional analyses for this sample suite are planned [K. Johnson, personal communication, 1992]. Twenty new K-Ar age determinations were also performed for emergent samples from the island of Ua Huka [H. Barsczus, personal communication, 1991].

Chemical Variability of Marquesan Basalts

Previous studies of Marquesas Islands samples [*Bishop and Woolley*, 1973; *Liotard et al.*, 1986; *Duncan et al.*, 1986; *Vidal et al.*, 1987] have documented a range in composition from tholeiitic to alkalic basalts, including compositions as evolved as trachytes and phonolites. Although quartz normative tholeiitic basalts (~1% quartz) are found on the islands of Ua Pou [*Liotard et al.*, 1986] and Eiao [*Caroff et al.*, 1990], most tholeiitic basalts from the Marquesas have olivine-normative compositions [*Liotard et al.*, 1986]. The tholeiitic basalts can be distinguished from alkalic basalts by lower rare earth element (REE) concentrations, especially in the light REEs, and by lower total incompatible element concentrations and ratios [*Liotard et al.*, 1986]. Isotopic composition does not uniformly correlate with major and trace element composition. In general, however, alkali basalts show more radiogenic Sr and moderately radiogenic Pb, and tholeiitic/transitional basalts have relatively unradiogenic Sr and variable Pb, indicating derivation from mantle sources with distinct Sr/Rb and U/Pb histories [*Dupuy et al.*, 1987].

The distribution of basalt compositions along the lineament gives a picture of the general petrologic development of a Marquesan volcano. Drill holes through the volcanic pile on the northwesternmost (oldest) island of Eiao (Figure 1) have sampled moderately alkalic basalts in the upper 900 m and quartz-bearing tholeiites in the lower 100 m [*Caroff et al.*, 1990]. Tholeiitic basalts have also been collected from the exposed shield areas that underlie the alkalic capping lavas of the central islands of Ua Pou [*Liotard et al.*, 1986], Nuku Hiva and Hiva Oa [*Duncan*, 1975]. In dredge hauls on two younger volcanoes, tholeiitic basalts have been recovered where only alkalic basalts had been found subaerially: at Tahuata (DH 19) and Fatu Hiva (DH 14) (Figure 1). Transitional basalts are often

found within the volcanic shield formed principally of tholeiitic basalts. A closer look at Fatu Hiva, the southeasternmost (youngest) island (Figure 1), shows that a full quarter of the volcanic edifice has collapsed below sea level. Deep submarine fault scarps bounding the flanks of this volcano have exposed tholeiitic (DH 14) and transitional basalts (DH 16). We combine these observations to conclude that the bulk of the submerged shield of a Marquesan volcano is composed of hypersthene-normative tholeiitic and transitional basalts that grade into, or are overlain after some break in volcanic activity by alkalic basalts. Sea Beam swath mapping [*McNutt et al.*, 1989] defined the location of several small cones southeast of Fatu Hiva, close to the inferred location of the hotspot. We cannot be certain if the composition of these cones (DH 12) represents the composition of the initial phase of Marquesan volcanism or if that initial phase is buried by DH 12 volcanism. Ages and chemical compositions suggest that DH 12 sampled only one flow.

Substantial crystal fractionation is indicated by the wide range of MgO content (11.16-2.52 wt %) and Mg numbers (67-37) [=100 $Mg^{+2}/(Mg^{+2}+Fe^{+2})$] (Tables 4 and 5) of the submarine lavas. None of the lavas, even the most primitive among the dredged samples, appear to have fractionated olivine alone. The more primitive lavas (Mg numbers >60) can be divided into three groups based on major and incompatible trace element concentrations, and Sr and Nd isotope ratios. The liquids parental to each of these three groups have resulted from variable melting conditions (depth, percent melting) of compositionally distinct sources. More evolved rocks can be related to these parental compositions by fractional crystallization of primarily olivine, clinopyroxene, and relatively less orthopyroxene and plagioclase (Figure 4). In Group I, the least fractionated lavas are tholeiitic basalts (DH 14, 19-1, 19-2); they are relatively depleted in incompatible elements and show unradiogenic isotope ratios, especially Sr. Based on major element compositions (49% SiO_2, 9.5% FeO, 2.0% Na_2O), the parental liquids for these lavas were generated by about 20% partial melting of somewhat depleted peridotite at 12 to 16 kbar pressure (40 to 60 km depth) [*Falloon et al.*, 1988]. The most primitive lavas of Group II are mildly alkalic or transitional in composition (DH 12, 17, 18, 19-3) and exhibit relatively unradiogenic isotopic ratios. Parental lavas for the strongly alkalic group, Group III (DH 22, 24) are relatively enriched in incompatible elements and have relatively radiogenic isotopic ratios. Parental liquids (43% SiO_2, 11.5% FeO, 2.8% Na_2O) for these lavas must have come from deeper than 60 km, after rather small degrees of partial melting (<5%) [*Falloon et al.*, 1988].

The drop in CaO/Al_2O_3 with decreasing Mg number (Figure 4) seen in the compositional trends for each group, indicates clinopyroxene fractionation. Although similar fractional crystallization paths are observed in all lava groups, the parental compositions in each group cannot be derived from one another by that process because of the diversity of CaO/Al_2O_3 at a given Mg number. Instead, variable degrees of partial melting of a mantle source with rather constant major element composition could produce the observed trend of decreasing CaO/Al_2O_3 with increasing Mg-number within the parental lavas within each group [e.g., *Falloon et al.*, 1988].

In a plot of Y versus Nb (Figure 5) parental lavas cluster into three groups, each similar to the other in Y content but with variable Nb content. Because isotopic ratios for each of the groups are different, variations in Nb, the more incompatible

TABLE 4. Major Element Analyses and CIPW-Normative Compositions for CRGN 02 Basalts

	12-1 FTI	12-6 FTI	12-10 FTI	12-11 FTI	12-12 FTI	12-17 FTI	14-1 FTI	16-1 FTI	16-2 FTI	16-3 FTI	17-1 FTI	17-2 FTI	17-5 FTI	18-13 MTN
					Major Element Analyses									
SiO_2	51.73	51.53	51.64	51.67	51.60	51.23	49.10	48.49	48.90	48.17	46.37	43.57	46.36	51.21
TiO_2	2.26	2.20	2.27	2.27	2.27	2.26	1.97	3.84	3.78	4.14	3.87	3.66	3.85	2.21
Al_2O_3	17.44	17.48	17.56	17.51	17.68	17.41	13.26	14.67	14.44	14.69	12.31	11.28	12.25	17.28
FeO	8.29	8.16	8.30	8.24	8.25	8.20	9.63	10.23	8.95	9.97	10.31	9.88	10.48	8.13
Fe_2O_3	1.38	1.36	1.38	1.37	1.38	1.37	1.44	1.53	1.34	1.50	1.72	1.65	1.75	1.36
MnO	0.20	0.20	0.20	0.20	0.20	0.20	0.14	0.15	0.12	0.16	0.16	0.16	0.16	0.22
MgO	2.84	2.93	2.52	2.77	2.89	2.89	11.16	6.54	7.57	5.73	9.63	9.59	9.99	2.91
CaO	7.19	7.01	7.20	7.19	7.17	7.17	10.01	8.79	9.90	10.17	9.53	8.98	9.50	7.00
Na_2O	4.98	4.74	5.23	4.98	4.92	4.97	2.42	3.18	2.72	2.82	2.53	2.33	2.57	4.92
K_2O	2.54	2.82	2.55	2.58	2.56	2.85	0.57	1.55	1.16	1.26	1.80	1.66	1.78	2.79
P_2O_5	1.28	1.25	1.32	1.29	1.29	1.29	0.21	0.69	0.41	0.50	0.53	0.50	0.53	1.27
Total	100.13	99.69	100.17	100.07	100.11	99.85	99.76	99.50	99.16	98.96	98.76	93.26	99.22	99.29
Mg number	38	39	39	37	38	39	65	50	48	57	62	63	60	39
					CIPW-Normative Compositions									
or	15.01	16.67	15.07	15.25	15.13	16.87	3.37	9.16	6.86	7.45	10.64	9.82	10.52	16.49
ab	37.01	35.75	36.68	36.89	36.84	33.77	20.48	26.91	23.02	23.86	19.14	17.27	18.37	34.84
an	17.73	17.98	16.91	17.81	18.60	16.81	23.64	21.18	23.77	23.70	16.92	15.42	16.63	16.83
ne	2.78	2.36	4.10	2.85	2.60	4.53	0	0	0	0	1.23	1.32	1.83	3.68
lc	0	0	0	0	0	0	0	0	0	0	0	0	0	0
di	8.05	7.24	8.59	7.93	7.17	8.72	19.95	14.66	18.35	19.24	21.75	20.92	21.87	8.06
hy	0	0	0	0	0	0	11.79	6.00	11.84	9.02	0	0	0	0
ol	10.45	10.60	9.45	10.07	10.58	10.20	14.38	10.64	5.39	4.64	18.01	18.21	19.12	10.46
mt	1.83	1.97	2.00	1.99	2.00	1.81	2.09	2.22	1.94	2.17	2.49	2.18	2.13	1.79
il	4.29	4.18	4.31	4.31	4.31	4.30	3.74	7.29	7.18	7.86	7.35	6.95	7.31	4.20
ap	3.03	2.96	3.12	3.05	3.05	3.06	0.50	1.63	0.97	1.18	1.25	1.18	1.25	3.01
Group	II	II	II	II	II	II	I	II	II	II	II	II	II	II
Type	KT	KT	KT	KT	KT	KT	OT	B	B	B	AOB	AOB	AOB	KT

	18-26 MTN	18-40 MTN	19-1 THU	19-2 THU	19-3 THU	19-8 THU	19-11 THU	21-8 DMD	21-14 DMD	22-1 UAP	22-2 UAP	22-3 UAP	24-4 UAP	24-7 UAP	24-8 UAP
					Major Element Analysis										
SiO_2	47.92	47.40	48.25	48.34	47.48	45.07	48.33	48.68	47.59	43.43	42.88	43.43	44.58	44.35	44.29
TiO_2	3.76	3.37	2.93	2.91	3.19	3.73	3.82	3.57	4.09	3.46	3.31	3.33	3.37	3.42	3.38
Al_2O_3	12.23	13.06	12.02	11.81	11.30	13.74	14.74	15.50	15.30	12.92	12.57	12.81	15.12	15.04	15.47
FeO	10.15	9.96	10.47	10.08	9.91	10.92	10.01	10.38	11.39	11.26	11.48	11.55	10.41	10.56	10.21
Fe_2O_3	1.52	1.49	1.57	1.51	1.49	1.64	1.50	1.56	1.71	1.69	1.72	1.73	1.56	1.58	1.53
MnO	0.17	0.30	0.20	0.16	0.16	0.18	0.18	0.19	0.19	0.23	0.20	0.26	0.22	0.22	0.20
MgO	10.00	9.48	10.06	9.93	11.30	7.55	5.28	4.05	4.58	9.92	10.26	9.95	6.10	5.87	5.56
CaO	10.42	9.24	10.56	10.53	10.40	10.91	10.03	8.42	9.26	12.30	11.70	11.91	10.02	9.93	9.77
Na_2O	2.56	2.99	2.09	2.08	2.32	3.20	2.69	4.07	3.58	2.53	2.69	2.82	4.07	4.52	4.20
K_2O	1.22	1.77	0.88	0.95	1.19	2.78	1.95	1.75	1.37	1.86	1.93	1.96	3.09	3.16	3.25
P_2O_5	0.52	0.56	0.34	0.34	0.40	0.65	0.55	0.78	0.77	0.45	0.43	0.43	0.75	0.76	0.78
Total	100.47	99.62	99.37	98.64	99.14	100.37	98.92	98.95	99.83	100.05	99.17	100.17	99.29	99.41	98.65
Mg number	64	63	63	64	67	56	46	41	42	61	62	61	51	50	50
					CIPW-Normative Compositions										
or	7.21	10.46	5.20	5.61	7.03	16.43	11.52	10.34	8.10	10.99	9.71	10.04	18.26	18.67	19.21
ab	21.66	20.76	17.69	17.60	19.63	4.14	22.76	31.35	29.28	0.04	0	0	3.08	1.32	2.68
an	18.28	16.99	20.82	20.08	16.91	14.92	22.39	18.86	21.63	18.40	16.52	16.51	13.86	11.42	13.76
ne	0	2.46	0	0	0	12.43	0	1.68	0.55	11.58	12.33	12.93	16.99	20.01	17.80
lc	0	0	0	0	0	0	0	0	0	0	1.33	1.21	0	0	0
di	24.25	20.41	23.81	24.26	25.86	28.58	19.57	14.84	16.03	32.24	31.46	32.37	25.46	27.09	24.41
hy	2.41	0	13.34	14.28	2.80	0	5.12	0	0	0	0	0	0	0	0
ol	16.10	18.68	9.88	8.30	17.97	12.92	7.01	11.04	12.22	16.73	18.04	17.30	11.25	10.36	10.34
mt	2.21	2.16	2.28	2.19	2.16	2.37	2.17	2.26	2.48	2.45	2.50	2.51	2.26	2.29	2.22
il	7.14	6.40	5.56	5.53	6.06	7.08	7.26	6.78	7.77	6.57	6.29	6.32	6.40	6.50	6.42
ap	1.23	1.33	0.80	0.80	0.95	1.54	1.30	1.85	1.82	1.07	1.02	1.02	1.78	1.80	1.85
Group	II	II	I	I	II	III	II	I	I	III	III	III	III	III	III
Type	B	AOB	OT	OT	B	BT	B	AOB	AOB	TE	TE	TE	BT	BT	BT

FTI = Fatu Hiva, MTN = Motu Nao, THU = Tahuata, DMD = Dumont D'Urville, UAP = Ua Pou, TH = tholeiitic series basalt, TR = transitional series basalt, ALK = alkali series basalt, OT = olivine tholeiite, B = basalt, AOB = alkali olivine basalt, KT = potassic trachyandesite, TE = tephrite, BT = basanite.

element, cannot be explained by only different degrees of partial melting of a single source and must reflect a range of source compositions for the primitive lavas. Linear trends exist between the primitive and more evolved lavas within each group that reflect fractionation of minerals in which both elements are equally incompatible.

Isotopic and Trace Element Compositions

Source heterogeneity has been implicated from trace element and isotopic compositions of island samples from the Marquesas lineament [*Liotard et al.*, 1986; *Duncan et al.*, 1986; *Dupuy et al.*, 1987; *Vidal et al.*, 1987]. The diversity of

TABLE 5. Electron Microprobe Analyses and CIPW-Normative Compositions for CRGN 02 Dredged Basalts

	12-10 FTI	14-1 FTI	16-1 FTI	17-1/5 FTI	18-20 FTI	18-60 FTI	19-1 FTI	19-7 FTI	21-1C DMD	21-1B DMD	22-3 UAP	22-5 UAP	24-1/7 UAP
					Electron Microprobe Analyses								
SiO_2	54.53	48.99	51.12	46.39	45.12	47.81	48.79	46.86	46.91	48.12	48.24	44.67	44.95
TiO_2	2.14	2.17	4.22	4.31	3.25	3.75	3.31	3.20	3.80	3.66	3.77	3.27	3.07
Al_2O_3	17.00	14.00	14.11	14.02	17.51	15.24	13.00	17.45	15.14	15.50	15.43	17.51	17.17
FeO^*	8.26	9.65	11.23	11.27	10.46	10.51	11.42	10.05	11.88	11.81	10.70	10.28	9.63
MnO	0.20	0.14	0.15	0.16	0.24	0.14	0.14	0.13	0.20	0.19	0.15	0.20	0.21
MgO	3.14	6.43	3.82	5.27	3.90	4.69	5.86	3.35	4.69	4.55	4.19	3.88	3.63
CaO	6.36	10.07	7.92	10.91	10.20	11.13	8.57	8.57	8.88	8.73	9.64	10.11	9.30
Na_2O	4.60	2.82	2.79	3.11	3.97	3.37	2.53	3.75	3.63	3.12	3.37	4.20	4.43
K_2O	2.67	0.56	2.43	1.43	2.98	2.00	0.88	3.20	1.37	1.54	2.06	3.17	3.74
P_2O_5	0.91	0.23	0.91	0.51	0.60	0.50	0.34	0.88	0.58	0.58	0.56	0.59	0.72
Total	96.93	96.99	97.30	98.70	98.23	97.38	98.33	98.14	97.08	97.80	98.10	97.88	96.93
Mg number	44	50	41	49	44	48	41	44	45	44	45	44	44
					CIPW-normative compositions								
Q	0.00	0.00	4.24	0.00	0.00	0.00	0.22	0.00	0.00	0.00	0.00	0.00	0.00
Or	15.76	3.31	14.34	0.44	17.59	11.80	5.19	23.02	8.09	9.09	12.16	18.71	22.07
Ab	38.73	23.84	23.59	22.17	7.34	23.01	21.39	13.06	28.87	26.38	26.02	4.64	4.27
An	18.07	26.06	18.79	20.06	21.15	20.53	23.69	19.26	20.96	23.72	20.88	19.56	15.91
Ne	0.09	0.00	0.00	2.24	14.21	2.97	0.00	10.10	0.99	0.00	1.34	16.73	17.99
Di	6.23	21.46	11.99	25.08	21.06	21.67	23.96	14.5	15.90	13.01	19.19	22.05	21.38
Hy	0.00	12.54	13.08	0.00	0.00	0.00	14.00	0.00	0.00	10.25	0.00	0.00	0.00
Ol	9.94	2.59	0.00	7.50	6.93	7.51	0.00	7.82	11.05	2.13	7.67	0.00	5.62
Mt	1.85	2.17	2.53	2.53	2.36	2.36	2.57	2.26	2.68	2.26	2.4	2.31	2.17
Il	4.07	4.13	8.03	8.20	6.18	7.13	6.30	6.09	7.23	6.96	7.17	6.22	5.84
Ap	2.10	0.23	2.10	1.18	1.39	1.34	0.79	2.03	1.34	1.34	1.27	1.36	1.66
Group	II	I	II	II	II	II	I	III	II	II	III	III	III
Type	TA	OT	B	AOB	BT	AOB	QT	HAW	AOB	B	AOB	BT	BT

FTI = Fatu Hiva, THU = Tahuata, DMD = Dumont D'Urville, UAP = Ua Pou, TH = tholeiitiic series basalt, TR = transitional series basalt, ALK = alkali series basalt, QT = quartz tholeiite, OT = olivine tholeiite, B = basalt, AOB = alkali olivine basalt, TA = trachyandesite, BT = basanite, HAW = hawaiite.
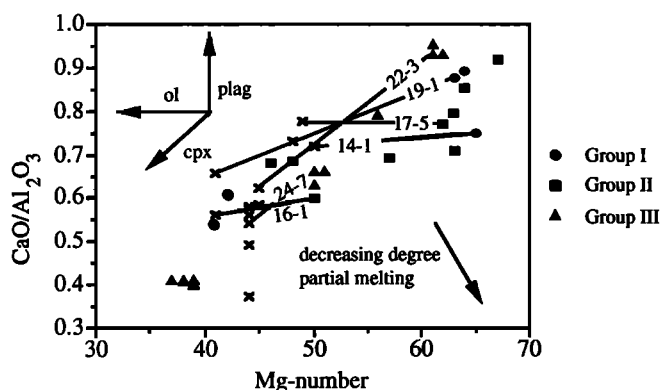

Fig. 4. CaO/Al_2O_3 versus Mg number for CRGN 02 lavas. Cross indicates composition of glasses, other symbols represent whole rock compositions. Lines are shown connecting whole rock and glass compositions from the same sample with sample number on the connecting line. Where the most primitive compositions within a trend are tholeiitic, those lavas and their possible differentiates are called Group I; where the most primitive compositions within a trend are mildly alkalic, those lavas and their possible differentiates are called Group II. Group III refers to primitive alkalic lavas and their possible differentiates. Directions of the change of liquid compositions with olivine (ol), clinopyroxene (cpx), and plagioclase (plag) removal are shown. Arrow indicates the compositional change of liquids with decreasing degree of partial melting of a single homogeneous source. Rocks and their glasses are related by crystal fractionation. All lavas appear to have undergone ol and some cpx removal except DH 17-5 which has had olivine removal only.
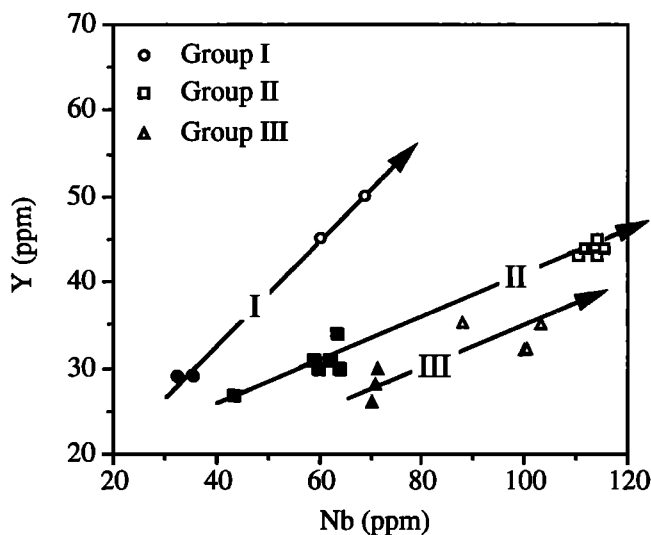

Fig. 5. Y (ppm) versus Nb (ppm) for CRGN 02 basalts. Arrows show fractionation relationships within the three compositional groups as described in Figure 4. Solid symbols represent lavas with Mg number >60.

incompatible trace elements, reported in Table 6, and radiogenic isotope ratios (Table 7) found in CRGN 02 dredged samples supports this idea [*Desonie*, 1990]. Within the submarine sample suite $^{87}Sr/^{86}Sr$ ranges from 0.70328 to 0.70551, and the total Sr isotopic variation within the

Marquesas lineament is nearly as great as in all OIB globally. A similarly large variation is found in $^{143}Nd/^{144}Nd$, but a much smaller range is found in Pb isotope ratios. A plot of εNd versus $^{87}Sr/^{86}Sr$ for Marquesan samples (Figure 6a) demonstrates that the tholeiitic basalts have less radiogenic Sr than the transitional and alkalic basalts. Although tholeiitic and alkalic basalt isotopic compositions are distinct, mixing between two sources is prevalent. At Ua Pou and Tahuata (DH 19) tholeiitic/transitional and alkalic basalts are clearly separated in isotopic composition space, emphasizing the

TABLE 6. Trace Element Analyses for Samples Dredged on CRGN 02

	12-1 FTI	12-6 FTI	12-10 FTI	12-11 FTI	12-12 FTI	12-17 FTI	16-2 FTI	17-1 FTI	17-2 FTI	17-5 FTI	18-13 FTI	18-26 FTI	18-40 FTI
						XRF							
Ba	569	577	584	592	565	555		246	249	249	567	254	327
Cr	1	2	0	0	1	0	34	376	390	391	0	537	380
Cu	14	17	36	20	14	6		66	65	71	0	79	46
Ga	20	24	27	22	23	24		23	21	23	22	24	22
Nb	112	113	114	110	114	114		64	62	63	116	59	60
Ni	3	5	4	3	2	2		236	269	257	6	234	228
Pb	8	10	7	8	7	8		7	8	7	10	6	10
Rb	57	49	58	55	56	56		29	29	30	60	29	34
Sc	12	7	13	10	10	8		22	25	24	13	30	25
Sr	1231	1222	1247	1235	1225	1227		673	655	670	1225	605	783
Th	9	12	10	10	8	9		6	6	5	11	6	4
V	106	94	115	119	108	106		259	243	275	94	292	217
Y	44	44	43	43	45	44		30	31	34	44	31	30
Zn	132	137	155	132	133	128		120	123	122	133	112	128
Zr	439	460	452	439	448	459		289	282	289	464	276	316
						INAA							
Hf	12.2	12.4	11.5	12.3	12.5	12.2	7.7	6.6	8.1	7.5	12.1	7.1	8.4
La	93.9	91.8	92.6	95.2	93.5	91.0	36.7	34.6	44.0	43.5	94.8	44.9	48.8
Ce	198.6	199.9	187.4	190.8	196.2	192.7	85.3	69.8	92.9	92.0	188.8	85.2	103.0
Nd	98.2	103.0	98.9	97.2	96.6	93.5	47.7	37.9	47.1	50.4	89.8	43.9	64.2
Sm	16.5	15.2	16.3	16.4	16.1	15.5	8.1	8.3	9.3	9.4	16.0	9.2	10.6
Eu	5.07	4.96	4.90	5.07	5.17	5.02	2.94	2.72	3.14	3.35	4.90	3.02	3.37
Tb	1.55	1.94	1.61	1.58	1.43	1.68	0.88	0.95	1.18	1.27	1.59	1.01	1.12
Yb	3.39	3.10	3.57	2.71	2.86	2.84	1.94	1.96	1.68	2.05	3.32	1.91	2.45
Lu	0.43	0.40	0.45	0.42	0.44	0.46	0.18	0.25	0.23	0.25	0.39	0.26	0.42
(La/Sm)$_N$	3.51	3.72	3.51	3.58	3.58	3.63	2.93	2.85	3.66	3.93	3.85	3.66	3.01
Group	II	II	II	II	II	II	II	II	II	II	II	II	II
Type	M	M	M	M	M	M	B	AOB	AOB	AOB	M	B	AOB

	19-1 THU	19-2 THU	19-3 THU	19-8 THU	21-8 DMN	21-14 DMN	22-1 UAP	22-2 UAP	22-3 UAP	24-4 UAP	24-7 UAP	24-8 UAP
						XRF						
Ba	133	144	262	616	311	263	557	525	562	709	743	755
Cr	522	522	711	147	3	4	406	392	355	117	124	99
Cu	75	73	82	49	41	14	11	16	31	28	28	28
Ga	18	17	20	22	30	26	20	18	21	23	21	23
Nb	32	35	43	88	69	60	72	71	70	100	100	103
Ni	234	224	296	110	8	0	145	148	153	54	51	40
Pb	6	4	6	8	6	8	7	7	8	7	12	10
Rb	19	19	29	77	27	21	55	59	61	85	88	91
Sc	32	28	31	27	16	22	35	31	29	23	19	21
Sr	436	435	504	820	877	873	710	685	684	947	952	1002
Th	3	2	6	10	2	5	8	8	9	10	12	11
V	259	256	267	307	238	280	353	339	338	267	268	266
Y	29	29	27	35	50	45	30	28	26	32	32	35
Zn	104	96	108	120	169	154	103	102	107	114	116	118
Zr	198	199	221	331	447	394	201	199	199	302	301	315
						INAA						
Hf	6.7	5.0	6.0	9.5	12.4	11.3	5.7	5.5	5.9	7.5	7.7	8.0
La	32.7	25.4	33.6	81.2	49.4	43.2	67.6	59.4	61.8	77.2	86.0	78.2
Ce	69.3	49.7	67.7	151.0	109.8	98.1	111.1	103.7	102.5	145.5	154.7	153.8
Nd	41.6	29.3	43.3	76.5	81.6	77.4	54.4	49.2	47.8	72.9	67.1	62.6
Sm	8.1	6.5	7.2	10.9	16.0	14.2	8.1	8.2	8.3	10.0	10.4	10.1
Eu	2.52	2.16	2.46	3.54	5.33	4.80	2.64	2.48	2.33	2.96	3.22	3.12
Tb	1.01	0.97	0.98	1.51	1.94	1.64	1.03	0.92	1.06	1.05	1.00	1.20
Yb	1.90	1.91	1.55	2.57	3.09	2.95	2.55	2.20	2.55	2.40	2.31	2.92
Lu	0.28	0.29	0.18	0.26	0.42	0.38	0.29	0.29	0.28	0.29	0.30	0.39
(La/Sm)$_N$	2.48	2.42	2.86	4.58	1.91	1.88	5.12	4.47	4.58	4.76	5.09	4.76
Group	I	I	II	III	I	I	III	III	III	III	III	III
Type	OT	OT	B	BT	AOB	AOB	TE	TE	TE	BT	BT	BT

FTI = Fatu Hiva, THU = Tahuata, DMD = Dumont D'Urville, UAP = Ua Pou, OT = olivine tholeiite, B = basalt, AOB = alkali olivine basalt, M = mugearitic basalt, TE = tephritic basalt, BT = basanatic basalt.

close physical proximity of the sources for the two magma types, and their availability during construction of individual volcanoes. Closer inspection of the diagram reveals a significant geographic pattern to the compositions. At constant εNd, the $^{87}Sr/^{86}Sr$ becomes more radiogenic across the Marquesas lineament, from southwest to northeast (Figure 6b). The presence of tholeiitic samples at all positions shows that this isotopic gradient is not strictly a function of the degree of partial mantle melting. Intriguingly, the cross lineament Sr-isotopic gradient at the southeast end of the Society chain [*Devey et al.*, 1990] is also increasingly radiogenic from southwest to northeast.

The same separation seen in Sr and Nd isotopic composition for Ua Pou and DH 19 also appears in $^{87}Sr/^{86}Sr$ versus $^{206}Pb/^{204}Pb$ (Figure 7a). In these diagrams, tholeiitic and some transitional samples plot near a mixing line between

TABLE 7. Sr, Nd and Pb Isotopic Compositions for CRGN 02 Basalts

	Group	Type	$^{87}Sr/^{86}Sr$	$^{143}Nd/^{144}Nd$	εNd	$^{206}Pb/^{204}Pb$	$^{207}Pb/^{204}Pb$	$^{208}Pb/^{204}Pb$
12-1	II	M	0.703737	0.512835	3.8	19.448	15.590	39.119
12-17	II	M	0.703753			19.444	15.554	39.025
14-1	I	OT	0.703490	0.512886	4.8	19.522	15.592	39.163
16-1	II	B	0.703909	0.512842	3.9	19.651	15.621	39.283
16-3	II	B	0.703473	0.512869	4.5	19.677	15.598	39.331
17-1	II	AOB	0.703650	0.512864	4.4	19.530	15.602	39.158
17-5	II	AOB	0.703628	0.512860	4.3	19.542	15.615	39.202
18-13	II	B	0.703759	0.512840	3.9	19.485	15.605	39.193
19-1	I	OT	0.703673	0.512875	4.6	19.334	15.535	38.867
19-3	II	B	0.704180	0.512818	3.5	19.260	15.571	39.257
19-8	III	BT	0.705506	0.512690	1.0	19.133	15.632	39.183
19-11	II	B	0.705198	0.512744	2.0	19.286	15.614	39.294
21-14	I	AOB	0.703276	0.512895	5.0	19.323	15.562	38.977
22-1	III	TE	0.704920	0.512700	1.2	19.146	15.620	39.086
22-2	III	BT	0.704915	0.512727	1.7			
24-4	III	BT	0.705042	0.512703	2.9	19.203	15.606	39.175
24-7	III	BT	0.704955			19.167	15.558	39.015
24-8	III	BT	0.705052	0.512714	1.5	19.218	15.624	39.240

TH = tholeiitiic series basalt, TR = transitional series basalt, ALK = alkali series basalt, OT = olivine tholeiite, B = basalt, AOB = alkali olivine basalt, M = mugearitic basalt, TE = tephritic basalt, BT = basanitic basalt. Values are relative to the following standards with 2σ error in parentheses: E&A = 0.708020 (3.093 x 10^{-5}), La Jolla = 0.511840 (6.693 x 10^{-5}), NBS 981: $^{206}Pb/^{204}Pb$ = 16.906 (0.016), $^{206}Pb/^{204}Pb$ = 15.448 (0.020), $^{208}Pb/^{204}Pb$ = 36.558 (0.109).
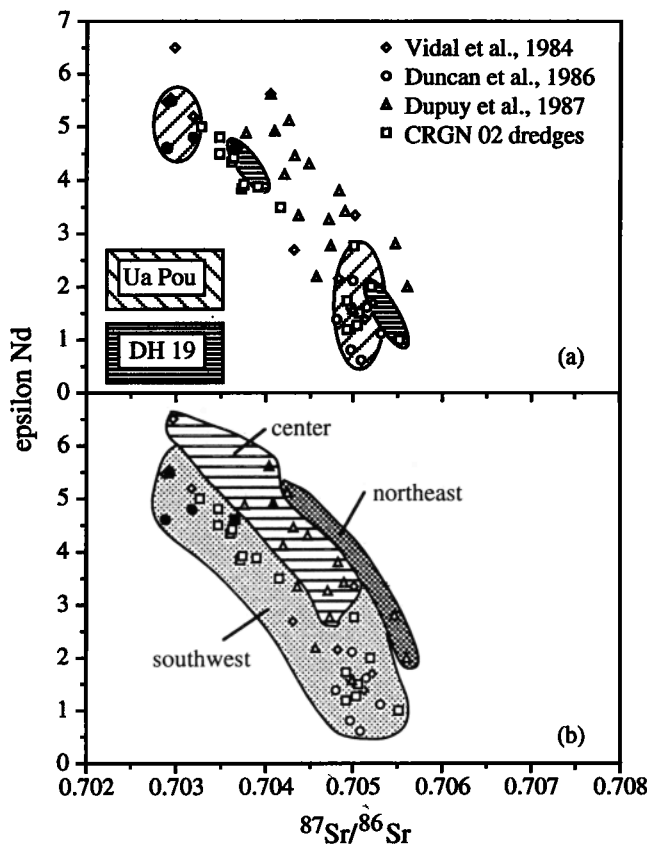
Fig. 6. Epsilon Nd versus $^{87}Sr/^{86}Sr$ for Marquesan basalts with (a) compositional fields for Ua Pou and DH 19 and (b) geographic trends across the volcanic lineament. Solid symbols indicate tholeiitic basalts. Major element data were not available for analyses of *Vidal et al.* [1984] so normative compositions could not be determined for these samples. Islands in the southwestern group of the lineament include Ua Pou, Dumont D'Urville, Tahuata, Motu Nao, Fatu Hiva, and the seamount at DH 12. The central group includes Eiao, Hatutu, Hiva Oa, and Motane; the northeastern group includes B^c J.Goguel, Ua Huka, and Fatu Huku.
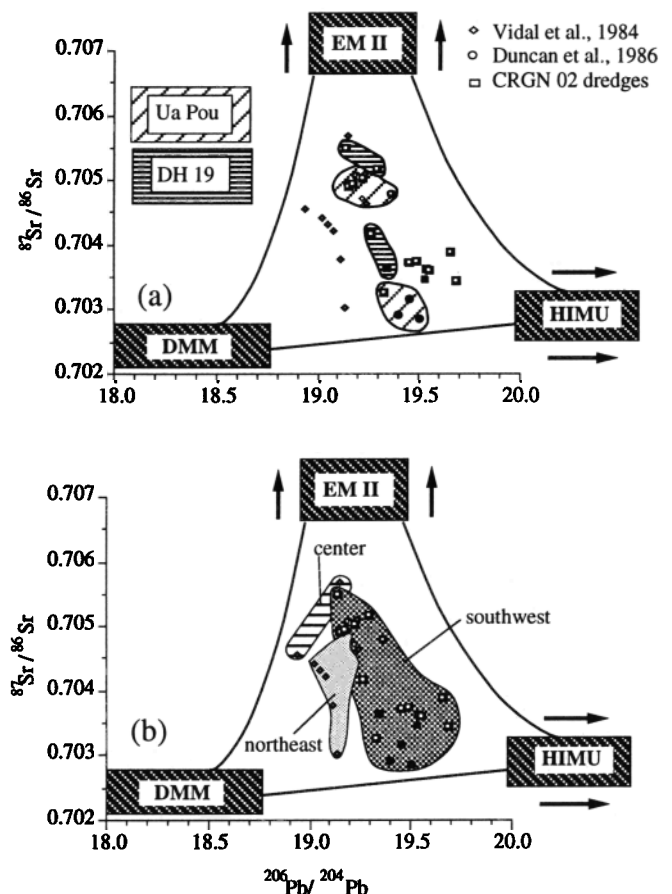

Fig. 7. $^{87}Sr/^{86}Sr$ versus $^{206}Pb/^{204}Pb$ for Marquesan basalts, with (a) compositional trends for Ua Pou and DH 19 and (b) geographic trends across the volcanic lineament. Tholeiitic basalts are shown by solid symbols. Islands are grouped geographically as described in Figure 5. Proposed compositions of mantle components from *Zindler and Hart* [1986] are shown in cross-hatched boxes.

DMM and HIMU while more alkalic compositions exhibit a strong EM II influence [*Dupuy et al.*, 1987]. It has been noted recently [*Hart et al.*, 1992] that lavas from many hotspot provinces define sublinear Sr-Nd-Pb isotopic arrays that converge toward depleted compositions, implying mixing between mantle plumes and the depleted upper mantle (asthenosphere and/or lithosphere). *Hart et al.* [1992] found that the depleted material in these mixing arrays, however, was not strictly DMM, but a composition falling between DMM and HIMU (which they termed FOZO, for "Focus Zone"), exactly as we see for the Marquesas array. In the present case the EM II component is more strongly expressed at lower degrees of partial melting. Thus either this component is ubiquitous and becomes diluted by the higher degrees of melting involved in producing the tholeiitic basalts, or it is derived from a spatially separate part of the hotspot that is tapped principally during the later volcanic stage of volcano construction. Both endmembers seem to be of regional significance. The first (DMM + HIMU) composition is seen at Easter Island, some of the Cook-Austral islands, the posterosional lavas at Tahiti [*Cheng et al.*, 1987; R. A. Duncan, unpublished data, 1987], as well as the Ua Pou tholeiites; the second (EM II) appears in the shield lavas at Samoa, the Society, the Marquesas, and some of the Cook-Austral Islands (Figure 2).

A geographic pattern to the isotopic variations can also be recognized in Figure 7b. Samples from the southwestern side of the Marquesas lineament show a larger HIMU component while the central samples are more EM II-like and the northeastern samples show more of a DMM component. Sampling in the Marquesas chain, however, has been biased toward the western region and the full compositional variability of the eastern region must await further studies.

Basalts from the CRGN 02 sample collection can also be distinguished in large-ion lithophile element ratio diagrams, such as Zr/Nb versus (La/Sm)$_N$ (Figure 8), where Groups I, II and III are clearly separated. The trace element and isotopic variability is remarkably highly correlated: Group I lavas have high Zr/Nb, low La/Sm and low $^{87}Sr/^{86}Sr$, Group II lavas are
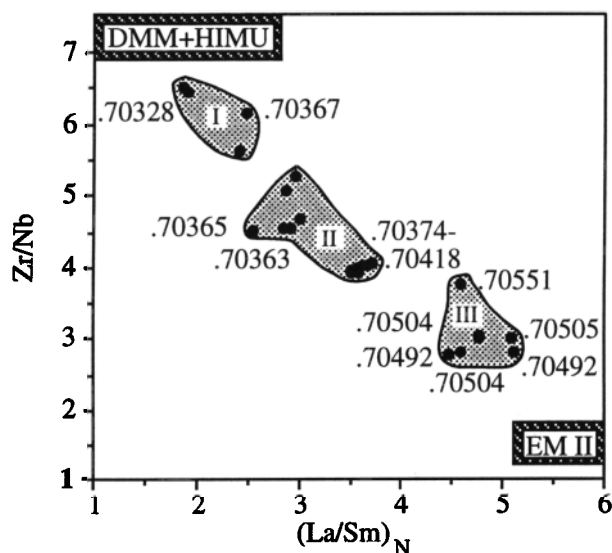
intermediate, and Group III lavas show the converse. Such a relationship is consistent with either melting of two compositionally distinct mantle sources (one generally DMM+HIMU-like, the other EM II-like), followed by mixing of the melts, or variable melting of a single source that is heterogeneous on a small length scale (kilometer or less). A general trend in incompatible element ratios across the lineament, complementary to the isotopic gradients, is also seen. For example, in an incompatible element ratio-ratio plot (Figure 9) the southwest and northeast groups of volcanoes show separate and distinct compositions, varying from a low Ba/La, high K/Rb component (eastern group) to a high Ba/La, low K/Rb component (western group). The central region appears to be a zone of mixing between the southwestern and northeastern compositions.

The covariation of isotopic and trace element ratios with mixing and degree of partial melting is further explored in Figure 10, where εNd is plotted against (La/Sm)$_N$. Isotopic ratios are not affected by variable melting or crystallization, whereas incompatible element ratios may be controlled, especially by melting. εNd values for hypothetical source endmembers for melting were chosen to match the composition of the most EM II-like basalt (DH 19-8) and an arbitrary composition between DMM and the most DMM+HIMU-like Ua Pou tholeiite [*Duncan et al.*, 1986]. The (La/Sm)$_N$ values for these endmembers were estimated from the same basalt compositions by considering ratios necessary to generate the basalts with less than 25% melting of spinel peridotite [*Falloon et al.*, 1988]. The (La/Sm)$_N$ ratios for hypothetical 2 to 25% equilibrium melts of these endmember sources were then calculated and displayed as mixing lines in Figure 10. The results show that the Marquesan melt compositions (corrected for low pressure crystal fractionation) can be accommodated by simple binary mixing of the two sources if degree of melting varies from 20% (tholeiites) to less than 2% (basanites).

Chondrite-normalized REE patterns show enrichments relative to MORB in all Marquesan basalts (Figure 11). Compositions vary rather smoothly from moderately light REE enriched (Group I, [La/Sm]$_N$=1.9 to 2.4) to strongly light REE enriched (Group III, [La/Sm]$_N$=4.5 to 5.1). Group I basalts have

Fig. 8. Zr/Nb versus (La/Sm)$_N$ with $^{87}Sr/^{86}Sr$ indicated for CRGN 02 lavas. Basalts of the three trends (Groups I, II, and III) cluster between EM II and DMM/HIMU components.
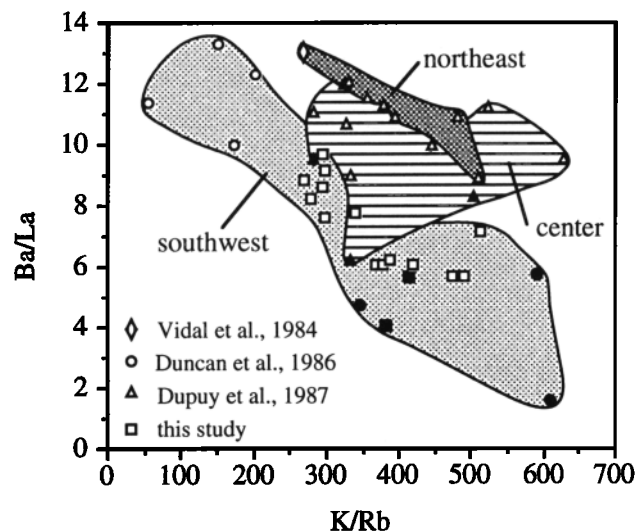

Fig. 9. Ba/La versus K/Rb with geographic trends across the volcanic lineament. Islands are grouped geographically as described in Figure 6. Tholeiitic basalts are shown by solid symbols.
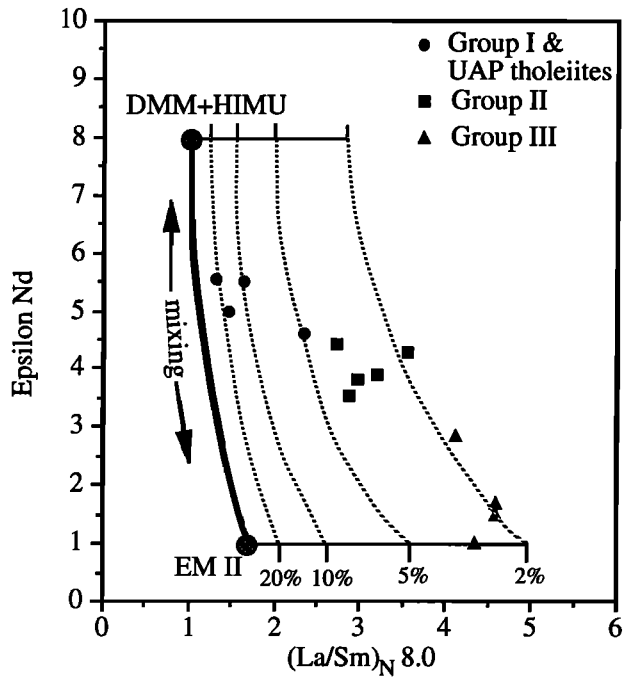
Fig. 10. Epsilon Nd versus (La/Sm)$_N$ for CRGN 02 basalts. To adjust for shallow level fractionation effects (La/Sm)$_N$ composition was calculated for parental liquids (Mg number = 65-70). Compositions for DMM+HIMU and EM II components are approximately εNd ~ 8, (La/Sm)$_N$ ~ 1, and εNd ~ 1, (La/Sm)$_N$ ~1.7, respectively. A mixing line for the components is shown. The horizontal lines indicate percent of partial melting of a DMM+HIMU or an EM II composition with curved lines connecting equivalent degrees of melting. Tholeiitic samples are the result of higher degrees of melting of a more dominantly DMM+HIMU source; alkalic samples derive from lower degrees of melting of a more EM II-like source.
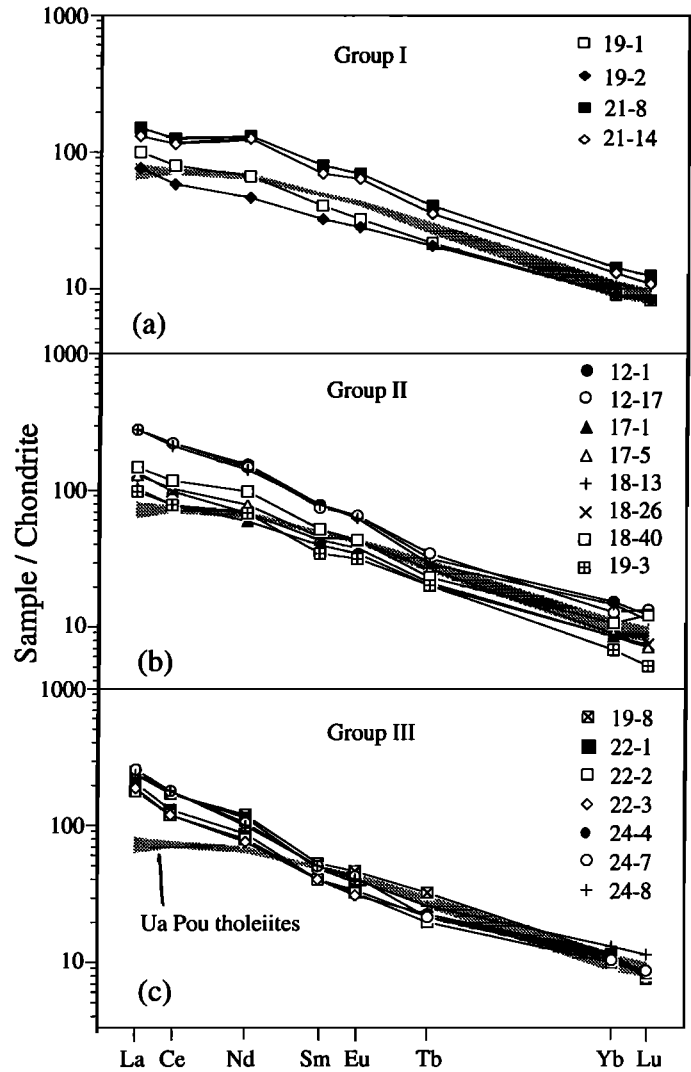

Fig. 11. REE patterns for all Marquesas dredged samples: (a) pattern for Group I trend lavas, (b) pattern for Group II trend lavas, (c) pattern for Group III trend lavas. Chondrite normalized after Nakamura [1974]. REE patterns for tholeiitic basalts from the island of Ua Pou are shown as a dotted field.

patterns very similar to the Ua Pou tholeiites (field shown by Liotard et al. [1986]); the slightly concave-downward light REE portion is reminiscent of Hawaiian tholeiites [e.g., Budahn and Schmitt, 1985]. The progressive fanning of these patterns to higher light REE contents at approximately constant heavy REE contents from Group I to II to III is consistent with decreasing partial melting of peridotite within the spinel to garnet stability fields. A few of the more primitive Group II lavas (e.g., 19-3) show lower heavy REE contents than the Ua Pou tholeiites, and the Group III lavas show patterns with slight concave-upward curvature, indicative of garnet control during melting. All the Group III lavas, largely basanites, are evolved (Mg number 50-62) and their primitive melts would have had significantly lower heavy REE contents, reflecting residual garnet in the region of melting. Within each group patterns are easily related by fractional crystallization, dominantly of olivine and clinopyroxene, consistent with the major element fractionation paths (Figure 4). The lack of any significant Eu anomaly suggests that plagioclase addition or removal was not a major factor in the petrogenesis of these suites.

DISCUSSION

Volcanism that has built the Marquesas lineament is understandable in terms of Pacific plate motion across a quasi-stationary hotspot, maintained by a plume of upwardly convecting mantle. The individual islands and seamounts of this chain show a clear age progression and orientation

generally similar to other Pacific hotspot lineaments, and Marquesas basalt compositions fall within the range for hotspot-related volcanoes elsewhere in the Pacific Ocean basin, particularly the French Polynesian region. Several aspects of this volcanic province are remarkable, however, and provide new clues about the dynamic behavior of plumes and the thermal structure of hotspots.

First, the Marquesas chain is short and began to grow only about 6 m.y. ago, in contrast with longer-lived and more vigorous activity over the Hawaiian and Easter hotspots, and, to a lesser extent, the Cook-Austral and Society hotspots. Some evidence suggests that the Marquesas hotspot was more active earlier (60 to 30 Ma) and produced volcanoes through the region of the central Line Islands [Crough and Jarrard, 1981; Schlanger et al., 1984], on strike from the Marquesas Islands in the direction of Pacific plate motion. In this case, the plume flux must have varied considerably, perhaps in conjunction with changing vulnerability of the overlying lithosphere to melt penetration [Pollack et al., 1981; McNutt et al., 1989]. Buoyancy flux calculations of Sleep [1990] would suggest that

the Marquesas plume is one of the most vigorous in the ocean basins. His estimate was made by determining the buoyancy flux for the entire South Pacific Superswell and dividing the value by the number of hotspots (5) found within the Superswell [*Sleep*, 1990]. However, the Superswell is not caused by the coalescing of the individual hotspot swells within the region; abundant hotspot volcanism is found within the Superswell possibly because the lithosphere was previously warmed, allowing it to be penetrated by the hotspots [*McNutt and Fischer*, 1987]. Therefore calculating the buoyancy flux of a single hotspot in this manner would seriously overestimate the value for that hotspot. The Superswell may, in fact, be a longer-lived phenomenon than any of the hotspots currently found in the region [*Staudigel et al.*, 1991; *Larson*, 1991].

Second, the orientation of the chain is rotated clockwise about 30° from the direction expected from rigid Pacific plate motion over a hotspot that is fixed with respect to other Pacific basin hotspots [*Duncan and Clague*, 1985; *Gripp and Gordon*, 1990]. Coupled with this aberrant geometry, our best estimate of plate velocity across the hotspot (volcano migration rate) is significantly slower (by 30 mm/yr) than the rate expected from age determinations in other Pacific lineaments. *McNutt et al.* [1989] have proposed that the orientation of the Marquesas chain results from the coincidence of a limited region of weakness in the oceanic lithosphere located between the Marquesas and Galapagos fracture zones (Figure 1) and aligned parallel with the ancient spreading axis (NNW), and the path of a weak Marquesas hotspot. What could cause such a proposed "window" of vulnerability is unspecified. Because of the putative low plume flux and small melt production rates at this hotspot, magmas normally cannot penetrate the old, thick oceanic lithosphere. However, eastward sublithospheric flow from the hotspot as the more vulnerable section of Pacific lithosphere approached (6 Ma), direct vertical supply when the two coincided, and westward flow from the hotspot as the plate window receded (today) could produce a volcanic chain rotated

clockwise relative to the plate motion vector (Figure 12). The orientation would depend on the width of the "window" in the lithosphere and on how far plume material could flow from the hotspot to the vulnerable lithosphere. An alternative possibility (which we explore below) is that the weak Marquesas plume is more susceptible to shear by horizontal flow in the upper mantle and has been displaced to the southwest relative to stronger Pacific hotspots.

Third, we observe in the Marquesas basalts an unusually large range in isotopic compositions, which is strongly correlated with major and trace element contents. A common petrogenetic sequence in volcano construction is seen throughout the lineament, from tholeiitic and transitional lavas that consistently form the main shield-building volcanic phase, to terminal alkalic and basanitic lavas. (The composition of initial submarine eruptions is less clear, but mildly alkalic lavas are found at the site of most recent activity, DH 12.) Marquesan tholeiitic lavas are among the least radiogenic in Sr in Pacific islands, but show moderately radiogenic Pb, and reflect a mantle source composition lying on a mixing line between DMM and HIMU. Alkalic lavas, by contrast, show very radiogenic Sr and manifest melting of EM II mantle.

The major element variations result largely from the thermal structure and conditions of melting across the hotspot: tholeiitic magmas develop from relatively large degrees of mantle melting at shallow depths, while alkalic magmas derive from smaller degrees of melting at deeper levels [e.g., *Falloon et al.*, 1988]. REE patterns are consistent with this sequence and indicate melting progressing from the spinel to garnet stability fields with time. This presumably corresponds to the location of any individual volcano over the center and trailing edge, respectively, of the hotspot [*Duncan et al.*, 1986]. But while changes in the major element contents of magmas with time are controlled by phase equilibria of rather uniform peridotite composition, isotopic and, to a lesser extent, trace element compositions require melting of compositionally
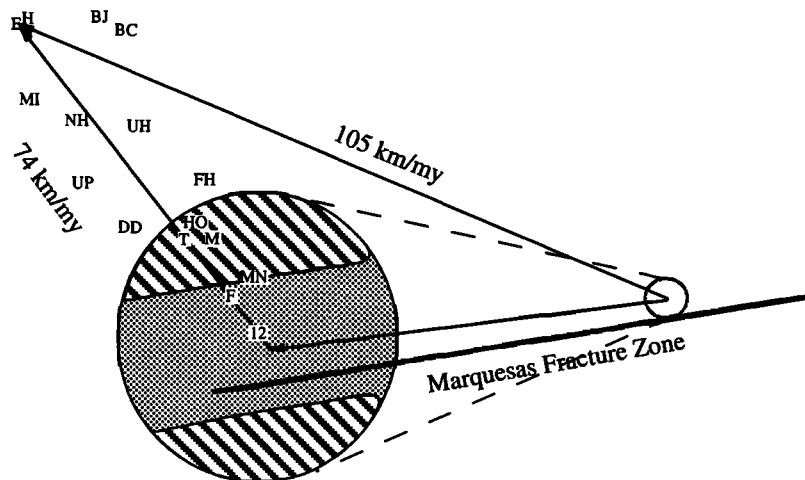

Fig. 12. Plan view of the Marquesas volcanic lineament showing the hypothetical effect of plume shear by westward upper mantle flow. The orientation of the chain is rotated 30° clockwise (74 km/m.y.) and the volcanic age progression is slower by 30 km/m.y., compared with that expected from fixed hotspots (105 km/m.y.). This feature, plus broadening of the melting region and inferred compositional segregation within the hotspot, could result from westward deflection of the plume and entrainment of upper mantle along the plume axis. Small circle is the location of the deep mantle root of the plume, dashed lines show direction of upper mantle shear, and shaded circle shows present hotspot, segregated by flow into plume (hachured) and upper mantle (gray stippling) compositions, as predicted from experiments by *Griffiths and Campbell* [1991]. The location of DR 12 is indicated by "12"; island locations shown as symbols as in Figure 3 with the addition of Bc Clark (BC), Matu Iti (MI), Dumont D'Urville (DD), and Motu Nao (MN).

distinct mantle sources. These sources may be physically separate regions of the hotspot (center, periphery) or be intimately mixed and expressed by variable degrees of melting.

How can we account for these aspects of the temporal, spatial and compositional variability of Marquesan volcanism? We consider three possible models:

1. All compositional variations are contained within a heterogeneous, but well-mixed plume. These heterogeneities may be primordial or acquired through subduction of altered oceanic lithosphere and sediments with variable Rb/Sr, U/Pb and Sm/Nd, and accumulation in the deep mantle over very long time scales [*White and Hofmann*, 1982]. Magma compositions are then controlled through variable partial melting of the heterogeneous plume. That is, the lower melting fractions (EM II-like, alkalic) dominate at low degrees of partial melting (hotspot edge), while the more residual material (DMM-like, tholeiitic) dominates at higher degrees of partial melting (hotspot center), following the "plum-pudding mantle" rationale for melting-composition correlations for EPR basalts [*Zindler et al.*, 1984]. We cannot, however, propose any strong argument why the HIMU component (long-term enrichment of U over Pb) should be associated with DMM and larger degrees of partial melting.

2. The plume has a uniform composition (EM II) and, over cooler parts of the hotspot, this composition dominates melts. Over the center of the hotspot higher temperatures lead to assimilation and melting of the lower lithosphere, which dominates magma compositions. The lower lithosphere must then have DMM+HIMU composition. Some support for this idea comes from detailed studies of EPR basalts [*White et al.*, 1987; *Graham et al.*, 1988], where Pb isotopic compositions appear to streak from DMM toward HIMU (Figure 2). Hence material added to the lower oceanic lithosphere as the plate cools and thickens could contain both DMM and HIMU components. However, unlike Hawaii, where posterosional lavas are isotopically depleted but LREE-enriched so small degrees of melting of oceanic lithosphere can be invoked to explain their origin [*Chen and Frey*, 1983], the amount of lithosphere necessary to produce the LREE-depleted and isotopically depleted shield lavas in the Marquesas would be enormous. Geophysical evidence regarding significant lithospheric melting is equivocal. *Fischer et al.* [1986] estimated a compensation depth of 45 ± 5 km for loading of the Marquesas volcanoes, implying convective thinning of the base of the underlying lithosphere. *Calmant and Cazenave* [1987] calculated an elastic thickness for the lithosphere under the Marquesas somewhat thinner than the global trend, and concluded that weakening by thermal erosion had occurred. In the most recent analysis of gravity and bathymetric data, however, *McNutt et al.* [1991] claim to detect no thinning or weakening of the oceanic lithosphere beneath the Marquesas region.

3. The plume is EM II composition, but is weak (relatively cool and low buoyancy flux). Horizontal flow in the upper mantle, generally from spreading ridges toward subduction zones, will shear the plume [*Richards and Griffiths*, 1988] and in the process upper mantle (DMM+HIMU) will be warmed around a boundary layer and entrained into the axis of the plume [*Richards and Griffiths*, 1988; *Griffiths and Campbell*, 1991]. This produces a compositional segregation at the hotspot such that plume material (EM II) resides at the edges and upper mantle (DMM+HIMU) occupies the center. Temperatures will still be highest in the center of the hotspot, leading to the

largest degrees of melting (tholeiites), and cooler toward the edges, producing smaller degrees of melting (alkalic basalts and basanites). Plume flux may actually be irregular: the Marquesas chain could represent a small pulse of material with waning flux toward the present.

We can dismiss the first model, that all compositional diversity results from variable melting of an intrinsically heterogeneous plume. The sequence of melt compositions repeated at each volcano along the lineament seems to require too regular a distribution of heterogeneities within the plume; the spatial scale and relative proportion of components available for melting must have been nearly constant through the history of Marquesan volcanism. This seems unlikely in view of the difficulty of thorough subsolidus mixing of subducted material, even on billion-year time scales [*Gurnis and Davies*, 1986]. Also, we would expect isotopic compositions to lie on mixing lines between low melting fraction material (EM II and HIMU) and residual material (DMM). Instead, the apparent mixing line identifies EM II and DMM+HIMU as melting endmembers. The DMM+HIMU component reflects involvement of the upper mantle source for spreading ridge melting, as seen in the streaking from DMM toward radiogenic Pb compositions along the East Pacific Rise [*White et al.*, 1987] and in Easter Island lavas [*White and Hofmann*, 1982]. This composition is a common endmember for hotspot chains distributed throughout the Pacific basin (Figure 2) and points to an upper mantle contribution to melting in all cases [*White*, 1985; *Hart et al.*, 1992].

The remaining two models both acknowledge mixing of plume and upper mantle material. Assimilation and melting of the lower lithosphere over the center of the hotspot, and entrainment of upper mantle into the axis of the plume are difficult to distinguish because they produce identical spatial patterns in melt compositions. To explain the Ua Pou tholeiites by assimilation of lower lithosphere, however, would require greater than 1:1 proportions of oceanic lithosphere (composition of primary melts for EPR lavas [*White et al.*, 1987] and plume melts (primary melt composition from DH 19-8 + 15% olivine added). Given the more refractory composition (and higher melting temperatures) of the lower lithosphere compared with the plume material, it does not seem possible to dilute the plume melts to such an extent. This level of wholesale heating and erosion of the lower lithosphere should also be manifest in weakening of the plate under the volcanic chain [*Fischer et al.*, 1986; *Calmant and Cazenave*, 1987] but latest evidence denies this [*McNutt et al.*, 1991]. Large amounts of lithosphere melting are not consistent with the physical evidence for the intermittent and relatively small volcanic production over the Marquesas hotspot. *Woodhead* [1992] has proposed substantial lithosphere melting and mixing with plume melts to explain geochemical variability seen within the Marquesas Islands. Lithospheric melting is favored because of the very regular succession of distinct compositional changes at nearly every island along the chain, and an apparent correlation between the elapsed time between volcanic phases and the magnitude of the compositional shifts. According to *Woodhead* [1992], longer repose times should allow greater pooling of plume melts, which overcomes the assimilation of lithospheric melts. However, the long repose times indicate a waning plume flux which should lead to proportionally greater dilution by lithospheric melts. There is certainly no evidence that longer repose times lead to greater volumes of posterosional lavas.

Finally, we note that rocks from DH 19 show as great a compositional separation as at Ua Pou, yet are contemporaneous (i.e., no repose time), so melts of extreme compositions were available for eruption at the same time, at least at Tahuata.

On the other hand, upper mantle material stirred into the axis of the plume would occupy the hottest part of the hotspot and is expected to be associated with the largest degree of partial melting. The *Griffiths and Campbell* [1991] analysis of sheared plumes is also instructive with regard to the orientation and timing of Marquesan volcanism. We have noted the 30° departure of the lineament from the orientation expected if the hotspot were fixed with respect to other Pacific hotspots. What if the buoyancy flux in the Marquesas plume has been weak and intermittent, so that local upper mantle flow has bent the plume toward the southwest? The required flow direction is roughly parallel with the old fracture zones, i.e., relative plate motion. In this case the plume flux has waned since the time of the beginning of the Marquesan chain (6 Ma) and the plume has been progressively deflected to the southwest (Figure 12). This would account for the orientation and smaller apparent plate velocity over the hotspot.

The magnitude of plume shearing and upper mantle entrainment is dependent on plume buoyancy flux. For a moderate buoyancy flux of 10^4 Ns^{-1}, plume bending of 20° from vertical, and reasonable initial (lower mantle) temperature anomaly ($\Delta T = 200\text{-}400°C$), Griffith and Campbell's calculations show that the ratio of entrained to plume material at the hotspot is about 2:1, the diameter of the hotspot should be 300-400 km, and the temperature anomaly over the hotspot is 70-140°C. Thus entrainment increases the volume of the plume and broadens the region of melting, but cools temperatures over the hotspot. In the Marquesas the long duration of volcanic activity at individual islands implies a broad hotspot; e.g., the 2-3 m.y. period from shield to capping phases (Ua Pou) indicates a 150-200 km radius melting region. Excess temperatures of 100°C are more than sufficient to generate tholeiitic melts over the center of such a diluted hotspot [e.g., *Falloon et al.*, 1988].

While some small amount of lithospheric assimilation must occur as melts migrate from the hotspot through the plate, we conclude that this effect is small in the generation of these melts and that compositional segregation within the hotspot, derived from interaction of the weak plume with horizontal flow in the upper mantle, best accounts for the temporal and spatial variability of Marquesan volcanism. High resolution, time-space studies of the compositional evolution of volcanic chains produced over plumes with different buoyancy fluxes, on lithosphere of different ages and compositions, and at different plate velocities (variable shear) should allow a comprehensive assessment of the conditions of plume and asthenosphere/lithosphere interaction.

REFERENCES

Bishop, A. C., and A. R. Woolley, A basalt-trachyte-phonolite series from Ua Pu, Marquesas Islands, Pacific Ocean, *Contrib. Mineral. Petrol.*, *39*, 309-326, 1973.
Brousse, R., H. G. Barsczus, H. Bellon, J.-M. Cantagrel, C. Diraison, H. Guillou, and C. Leotot, Les Marquises (Polynésie française): Volcanologie, géochronologie, discussion d'un modéle de point chaud, *Bull. Soc. Geol. Fr.*, *8*, 933-949, 1990.
Budahn, J. R., and R. A. Schmitt, Petrogenetic modelling of Hawaiian tholeiitic basalts: A geochemical approach, *Geochim. Cosmochim. Acta*, *49*, 67-87, 1985.
Calmant, S., and A. Cazenave, Worldwide estimates of the oceanic lithosphere elastic thickness under volcanoes, *Nature*, *328*, 236-238, 1987.
Caroff, M., R. C. Maury, P. Vidal, G. Guille, and C. Dupuy, Eiao Island (Marquesas): Interactions between EM and HIMU reservoirs, paper presented at Volcanisme intraplaque. Le point chaud de la Reunion, Université de la Réunion, St. Denis-de-la-Reunion, November 12-19, 1990.
Castillo, P., The Dupal anomaly as a trace of the upwelling lower mantle, *Nature*, *336*, 667-670, 1988.
Chen, C. -Y., and F. A. Frey, Origin of Hawaiian tholeiite and alkalic basalt, *Nature*, *302*, 785-789, 1983.
Cheng, Q., J. D. MacDougall, G. W. Lugmair, and J. Natland, Temporal variation in isotopic composition at Tahiti, Society Islands (abstract), *Eos Trans. AGU*, *68*, 1521, 1987.
Crough, S. T., and R. D. Jarrard, The Marquesas-Line Swell, *J. Geophys. Res.*, *86*, 11,763-11,771, 1981.
Desonie, D. L., Geochemical expression of volcanism in an on-axis and intraplate hotspot: Cobb and Marquesas, Ph.D. thesis, 145 pp., Oreg. State Univ., Corvallis, 1990.
Desonie, D. L., and R. A. Duncan, The Cobb-Eickelberg seamount chain: Hotspot volcanism with MORB affinity, *J. Geophys. Res.*, *95*, 12,697-12,711, 1990.
Devey, C. W., F. Albarede, J. -L. Cheminee, A. Michard, R. Muhe, and P. Stoffers, Active submarine volcanism on the Society hotspot swell (West Pacific): A geochemical study, *J. Geophys. Res.*, *95*, 5049-5066, 1990.
Duncan, R. A., Linear volcanism in French Polynesia, Ph.D. thesis, 150 pp., Aust. Nat. Univ., Canberra, 1975.
Duncan, R. A., and D. A. Clague, Pacific plate motion recorded by linear volcanic chains, *The Ocean Basins and Margins*, vol. 7A, edited by A. E. Nairn et al., pp. 89-121, New York, 1985.
Duncan, R. A., and W. Compston, Sr isotopic evidence for an old mantle source region for French Polynesian volcanism, *Geology*, *4*, 728-732, 1976.
Duncan, R. A., and R. B. Hargraves, $^{40}Ar\text{-}^{39}Ar$ geochronology of basement rocks from the Mascarene Plateau, Chagos Bank, and Maldive Ridge, *Proc. Ocean Drill. Program, Sci. Results*, *115*, 43-51, 1990.
Duncan, R. A., and I. McDougall, Migration of volcanism with time in the Marquesas Islands, French Polynesia, *Earth Planet. Sci. Lett*, *21*, 414-420, 1974.
Duncan, R. A., and I. McDougall, Linear volcanism in French Polynesia, *J. Volcanol. Geotherm. Res.*, *1*, 197-227, 1976.
Duncan, R. A., M. T. McCulloch, H.G. Barsczus, and D.R. Nelson, Plume versus lithospheric sources for melts at Ua Pou, Marquesas Islands, *Nature*, *322*, 534-538, 1986.
Dupuy, C., P. Vidal, H. G. Barsczus, and C. Chauvel, Origin of basalts from the Marquesas Archipelago (south central Pacific Ocean): Isotope and trace element constraints, *Earth Planet. Sci. Lett.*, *82*, 145-152, 1987.
Dziewonski, A. M., and J. H. Woodhouse, Global images of the Earth's interior, *Science*, *236*, 37-48, 1987.
Falloon, T. J., D. H. Green, C. J. Hatton, and K. J. Harris, Anhydrous partial melting of a fertile and depleted peridotite from 2 to 30 kb and application to basalt petrogenesis, *J. Petrol.*, *29*, 1257-1282, 1988.
Farley, K., J. Natland, J. D. Macdougall, and H. Craig, He, Sr, and Nd isotopes in Samoan basalts: Evidence for enriched and undepleted mantle compositions (abstract), *Eos Trans. AGU*, *71*, 1669, 1990.
Feigenson, M. D., A. W. Hofmann, and F. J. Spera, Case studies on the origin of basalt, II, The transition from tholeiitic to alkalic volcanism on Kohala volcano, Hawaii, *Contrib. Mineral. Petrol.*, *84*, 390-405, 1983.
Filmer, P. E., and M. K. McNutt, Gravity and flexure in the Marquesas Islands (abstract), *Eos, Trans. AGU*, *71*, 1598, 1990.

Fischer, K. M., M. K. McNutt, and L. Shure, Thermal and mechanical constraints on the lithosphere beneath the Marquesas swell, *Nature*, *322*, 733-736, 1986.

Graham, D. W., A. Zindler, M. D. Kurz, W. J. Jenkins, R. Batiza, and H. Staudigel, He, Pb, Sr and Nd isotope constraints on magma genesis and mantle heterogeneity beneath young Pacific seamounts, *Contrib. Mineral. Petrol.*, *99*, 446-463, 1988.

Griffiths, R. W., and I. Campbell, On the dynamics of long-lived plume conduits in the convecting mantle, *Earth Planet. Sci. Lett. 103*, 214-227, 1991.

Gripp, A. E., and R. G. Gordon, Current plate velocities relative to hotspots incorporating the NUVEL-1 global plate model, *Geophys. Res. Lett., 17*, 1109-1112, 1990.

Gurnis, M., and G. F. Davies, Mixing in numberical models of mantle convection incorporating plate kinematics, *J. Geophys. Res., 91*, 6375-6395, 1986.

Hart, S. R., A large-scale isotope anomaly in the Southern Hemisphere mantle, *Nature, 309*, 753-757, 1984.

Hart, S., and A. Zindler, Constraints on the nature and development of chemical heterogeneities in the mantle, *Mantle Convection: Plate Tectonics and Global Dynamics*, edited by W. R. Peltier, pp. 261-387, Gordon and Breach, New York, 1989.

Hart, S. R., E. H. Hauri, L. A. Oschmann, and J. A. Whitehead, Mantle plumes and entrainment: Isotopic evidence, *Science, 256*, 517-520, 1992.

Hooper, P. R., The role of magnetic polarity and chemical analysis in establishing the stratigraphy, tectonic evolution, and petrogenesis of the Columbia River Basalts, *Mem. Geol. Soc. India, 3*, 362-376, 1981.

Katao, H., H. Morinaga, M. Hyodo, H. Inokuchi, J. Matsuca, and K. Yaskawa, Geomagnetic paleosecular variation and K-Ar ages in Hiva Oa island, Marquesas, French Polynesia, *J. Geomagn. Geoelectr., 40*, 703-714, 1988.

Kruse, S. E., Magnetic lineations on the flanks of the Marquesas swell: Implications for the age of the seafloor, *Geophys. Res. Lett., 15*, 573-576, 1988.

Larson, R. L., Latest pulse of Earth: Evidence for a mid Cretaceous superplume, *Geology, 19*, 547-550, 1991.

Laul, J. C., Neutron activation analysis of geological materials, *Atomic Energy Review, 17*, 603-695, 1979.

Liotard, J. M., H. G. Barsczus, C. Dupuy, and J. Dostal, Geochemistry and origin of basaltic lavas from Marquesas Archipelago, French Polynesia, *Contrib. Mineral. Petrol., 92*, 260-268, 1986.

McDougall, I., and R. A. Duncan, Linear volcanic chains - Recording plate motions? *Tectonophysics, 63*, 275-295, 1980.

McNutt, M. K., and K. M. Fischer, The South Pacific superswell, in *Seamounts, Islands, and Atolls, Geophys. Monogr. Ser.*, vol. 43, edited by B. H. Keating et al., pp. 25-34, AGU, Washington, D. C., 1987.

McNutt, M. K., K. M. Fischer, S. Kruse, and J. Natland, The origin of the Marquesas fracture zone ridge and its implication for the nature of hot spots, *Earth Planet. Sci. Lett., 91*, 381-393, 1989.

McNutt, M., D. Caress, J. Mutter, and R. Detrick, Thickness of the elastic plate beneath the Marquesas Islands: Why is it so much greater in value than elsewhere in French Polynesia? (abstract), *Eos Trans. AGU, 72*, 437, 1991.

McNutt, M. K., and A. V. Judge, The superswell and mantle dynamics beneath the South Pacific, *Science, 248*, 969-975, 1990.

Nakamura, N., Determination of REE, Ba, Mg, Na and K in carbonaceous and ordinary chondrites, *Geochim. Cosmochim. Acta, 38*, 757-775, 1974.

Nakamura, Y., and M. Tatsumoto, Pb, Nd, and Sr isotopic evidence for a multi-component source for rocks of Cook-Austral Islands and heterogeneities of mantle plumes, *Geochim. Cosmochim. Acta, 52*, 2909-2924, 1988.

Nishimura, C. E., and D. W. Forsyth, Anomalous Love-wave phase velocities in the Pacific: Sequential pure-path and spherical harmonic inversion, *Geophys. J. R. Astr. Soc., 81*, 389-407, 1985.

Palacz, Z. A., and A. D. Saunders, Coupled trace element and isotope enrichment in the Cook-Austral-Samoa islands, southwest Pacific, *Earth Planet. Sci. Lett., 79*, 270-280, 1986.

Pollack, H. N., I. G. Gass, R. S. Thorpe, and D. S. Chapman, On the vulnerability of lithospheric plates to mid-plate volcanism: Reply to comments by P. R. Vogt, *J. Geophys. Res., 86*, 961-966, 1981.

Richards, M. A., and R. W. Griffiths, Deflection of plumes by mantle shear flow: Experimental results and a simple theory, *Geophys. J., 94*, 367-376, 1988.

Richards, M. A., and R. W. Griffiths, Thermal entrainment by deflected mantle plumes, *Nature, 342*, 900-902, 1989.

Schlanger, S. O., M. O. Garcia, B. H. Keating, J. J. Naughton, W. W. Sager, J. A. Haggerty, J. A. Philpotts, and R. A. Duncan, Geology and geochronology of the Line Islands, *J. Geophys Res., 89*, 11,261-11,272, 1984.

Sleep, N. H., Hotspots and mantle plumes: Some phenomenology, *J. Geophys. Res., 95*, 6715-6736, 1990.

Smith, W. H. F., H. Staudigel, A. B. Watts, and M. S. Pringle, The Magellan seamounts, Early Cretaceous record of the South Pacific isotopic and thermal anomaly, *J. Geophys. Res., 94*, 10,501-10,523, 1989.

Staudigel, H., K.-H. Park, M. Pringle, J. L. Rubenstone, W. H. F. Smith, and A. Zindler, The longevity of the South Pacific isotopic and thermal anomaly, *Earth Planet. Sci. Lett., 102*, 24-44, 1991.

Vidal, P., C. Chauvel, and R. Brousse, Large mantle heterogeneity beneath French Polynesia, *Nature, 307*, 536-538, 1984.

Vidal, P., C. Dupuy, H. G. Barsczus, and C. Chauvel., Hétérogénetiés du maneau et origine des basaltes des Marquises (Polynésie), *Bull. Soc. Geol. Fr., 8*, 633-642, 1987.

White, W. M., Sources of oceanic basalts: Radiogenic isotope evidence, *Geology, 13*, 115-118, 1985.

White, W. M., and A. W. Hofmann, Sr and Nd isotope geochemistry of oceanic basalts and mantle evolution, *Nature, 296*, 821-825, 1982.

White, W. M., A. W. Hofmann, and H. Puchelt, Isotope geochemistry of Pacific mid-ocean ridge basalt, *J. Geophys. Res., 92*, 4881-4893, 1987.

White, W. M., M. M. Cheatham, and R. A. Duncan, Isotope geochemistry of Leg 115 basalts and inferences on the history of the Reunion mantle plume, *Proc. Ocean Drill. Program Sci. Results, 115*, 53-61, 1990.

Woodhead, J. D., Temporal geochemical evolution in oceanic intra-plate volcanics: A case study from the Marquesas (French Polynesia) and comparison with other hotspots, *Contrib. Mineral. Petrol., 111*, 458-467, 1992.

Woodhead, J. D., and M. T. McCulloch, Ancient seafloor signals in Pitcairn Island lavas and evidence for large amplitude, small length-scale mantle heterogeneities, *Earth Planet. Sci. Lett., 94*, 257-273, 1989.

Wright, E., and W. M. White, The origin of Samoa: New evidence from Sr, Nd, and Pb isotopes, *Earth Planet. Sci. Lett., 81*, 151-162, 1986.

Zindler, A., and S. Hart, Chemical geodynamics, *Annu. Rev. Earth Planet. Sci., 14*, 493-571, 1986.

Zindler, A., H. Staudigel, and R. Batiza, Isotope and trace element geochemistry of young Pacific seamounts: Implications for the scale of upper mantle heterogeneity, *Earth Planet. Sci. Lett., 70*, 175-195, 1984.

D. L. Desonie, Geochemistry Building, Lamont-Doherty Earth Observatory, Palisades, NY 10964.

R. A. Duncan, College of Oceanic and Atmospheric Sciences, Oregon State University, Corvallis, OR 97331.

J. H. Natland, Rosenstiel School of Marine and Atmospheric Sciences, University of Miami, Miami, FL 33149.